PALACKÝ UNIVERSITY OLOMOUC

Faculty of Science

Department of Physical Chemistry

Xenobiotic metabolism by cytochrome P450 2C9 mutants

BACHELOR THESIS

Author:	**Tomáš Medek**
Study program:	B1407 Chemistry
Field of study:	Ecochemistry
Form of study:	Full-time
Supervisor:	**RNDr. Karel Berka, Ph.D.**
Date of submission:	5/12/2014

UNIVERZITA PALACKÉHO V OLOMOUCI

Přírodovědecká fakulta

Katedra fyzikální chemie

Odbourávání cizorodých látek mutantními formami cytochromu P450 2C9

BAKALÁŘSKÁ PRÁCE

Autor:	**Tomáš Medek**
Studijní program:	B1407 Chemie
Studijní obor:	Ekochemie
Forma studia:	Prezenční
Vedoucí práce:	**RNDr. Karel Berka, Ph.D.**
Termín odevzdání práce:	12. 5. 2014

I would like to thank to V. Bazgier for his help with docking.

I hereby declare that this thesis is my own work and effort and that it has not been submitted anywhere for any award or degree. Where other sources of information have been used, they have been properly acknowledged.

Prohlašuji, že jsem předloženou bakalářskou práci vypracoval samostatně za použití citované literatury.

V Olomouci dne 12. 5. 2014

Bibliografická identifikace

Jméno a příjmení autora	Tomáš Medek
Název práce	Odbourávání cizorodých látek mutantními formami cytochromu P450 2C9
Typ práce	Bakalářská
Pracoviště	Katedra fyzikální chemie
Vedoucí práce	RNDr. Karel Berka, Ph.D.
Rok obhajoby práce	2014

Abstrakt — Cytochrom P450 2C9 (CYP2C9) je významný enzym katalyzující biotransformaci řady léčiv, jako například antikoagulantu (S)-warfarinu a jeho enanciomeru (R)-warfarinu a nesteroidních protizánětlivých léků (S)-flurbiprofenu a diklofenaku. Různé allely CYP2C9 se liší svou metabolickou aktivitou, v některých případech dokonce bez zjevného důvodu (např. bodová mutace I359L mimo aktivní místo). V této práci se snažíme objasnit rozdíly metabolické aktivity vybraných mutantů CYP2C9 pomocí nástrojů molekulárního modelování. Struktury nativní formy (wt) CYP2C9 a jeho pěti mutantů I359L, F476L, F114L, F114W a R97F byly připraveny z krystalové struktury. Léčiva vybraná rozsáhlou literární rešerší byla nadokována do rigidních snímků získaných z trajektorií 100ns dlouhých molekulárně dynamických simulací pomocí programu AutoDock Vina. Nejkratší vzdálenosti od nadokovaného ligandu k hemovému železu byly u wt formy od 2,9 Å do 3,6 Å. Oproti tomu nejkratší vzdálenosti z dokování do struktur mutantů byly většinou delší až po 6,3 Å. Klinicky významný pokles *3 alely (I359L) se zdá být způsoben zmenšením kavity v aktivním místě vlivem aminokyselin L361 a L362. Změny v aktivitách mutantů F114 a F476 se zdají být rovněž způsobeny změnami architektury aktivního místa, protože mutované aminokyseliny mění pozici, orientaci a funkci původních aminokyselin. Zásadní význam R97 při vazbě hemu vodíkovými vazbami byl potvrzen a struktury s mutací R97F se ukázaly jako nestabilní. Prokázali jsme, že molekulární modelování je schopno vysvětlit rozdílné aktivity různých variant CYP2C9.

Klíčová slova	cytochrom P450, 2C9, in silico, molekulární dynamika, docking
Počet stran	50
Počet příloh	1
Jazyk	Anglický

Bibliographical identification

Author's first name and surname   Tomáš Medek
Title   Xenobiotic metabolism by cytochrome P450 2C9 mutants
Type of thesis   Bachelor
Department   Department of physical chemistry
Supervisor   RNDr. Karel Berka, Ph.D.
The year of presentation   2014

Abstract   Cytochrome P450 2C9 (CYP2C9) is an important enzyme for biotransformation of various drugs such as anticoagulant (S)-warfarin and its enantiomer (R)-warfarin and NSAIDs (S)-flurbiprofen and diclofenac. Allelic variants of CYP2C9 differ in their metabolic activity in some cases with no obvious reason (eg. I359L point mutation). Here, we try to explain the variability of the CYP2C9 mutants with molecular modelling tools. Structures of wild type (wt) CYP2C9 and its five mutants I359L, F476L, F114L, F114W and R97F were prepared from crystal structure and they were equilibrated with 100ns-long molecular dynamics simulations. Selected drugs identified by extensive literature review were docked into the rigid snapshots acquired from trajectories with AutoDock Vina. The closest distances to heme iron from docking of ligand into wt active site ranged between 2.9 Å to 3.6 Å. Meanwhile, the closest distances from docking into mutant structures were usually longer up to 6.1 Å. Clinically important drop of activity of *3 allele (I359L) seems to be caused by the shrinking of the active site cavity due to the L361 and L362 amino acids. Changes in activity of mutants of F114 and F476 seems to be also caused by the redesign of active site cavity architecture as mutated residues changed the position, orientation and function of original residues. Key role of R97 in hydrogen bonding of heme propionates has been confirmed. We have shown, that the molecular modelling is able to explain the different activity of individual CYP2C9 variants.

Keywords   cytochrome P450, 2C9, in silico, molecular dynamics, docking
Number of pages   50
Number of appendices   1
Language   English

Content

Aims of the Thesis

➢ To provide literature review about effects of mutations on the cytochrome P450 2C9 substrate specificity.

➢ To prepare and validate models of selected mutants of cytochrome P450 2C9.

➢ To describe changes imposed on structure via mutations during 100 ns molecular dynamics simulation.

➢ To dock typical substrates into the structures of mutants to explain substrate specificity of cytochrome P450 2C9 mutants.

1 Theoretical Background

1.1 Cytochrome P450s

Cytochrome P450s, usually abbreviated as CYP, is one of the largest protein superfamilies. They catalyze wide range of reactions, but mostly oxidation, of many endogenous compounds as fatty acids, steroids or prostaglandins, as well as xenobiotics like products of plant secondary metabolism, environmental pollutants, agrochemicals and drugs (Anzenbacher and Anzenbacherová, 2001). They are heme enzymes and can be found across all species. Their name originates from highly typical absorption "Soret peak" at 450 nm upon reduction with carbon monoxide. CYP superfamily is divided into families named by abbreviation CYP followed by an Arabic numeral, which are further divided into subfamilies indicated by addition of capital letter. Individual proteins are then distinguished by secondary digit (e. g. *CYP3A4*). Due to their major role in the first phase of drug metabolism they are also studied for their connection with drug interactions and evaluation of proper dosage reflecting interindividual differences (Danielson, 2002; Miners and Birkett, 1998).

1.1.1 Reaction Cycle of CYP

Typical monooxygenation reaction can be denoted as:

$$R\text{-}H + O_2 + e^- \rightarrow R\text{-}O\text{-}H + H_2O \quad (1)$$
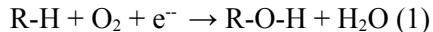
where R-H is substrate which has to traverse into the buried active site.

Substrate binds as sixth ligand to the heme iron replacing water. Ferric iron (Fe^{III}) is then reduced to a ferrous state (Fe^{II}) and binds oxygen molecule forming oxy-P450 complex, that is subsequently reduced to a peroxo-ferric intermediate and further protonated twice. This results in heterolysis of O-O bond. As a result, highly reactive ferrate (Fe^{IV}) radical is formed, which further oxidate the substrate (Denisov et al., 2005). See reactive cycle at Figure 1.
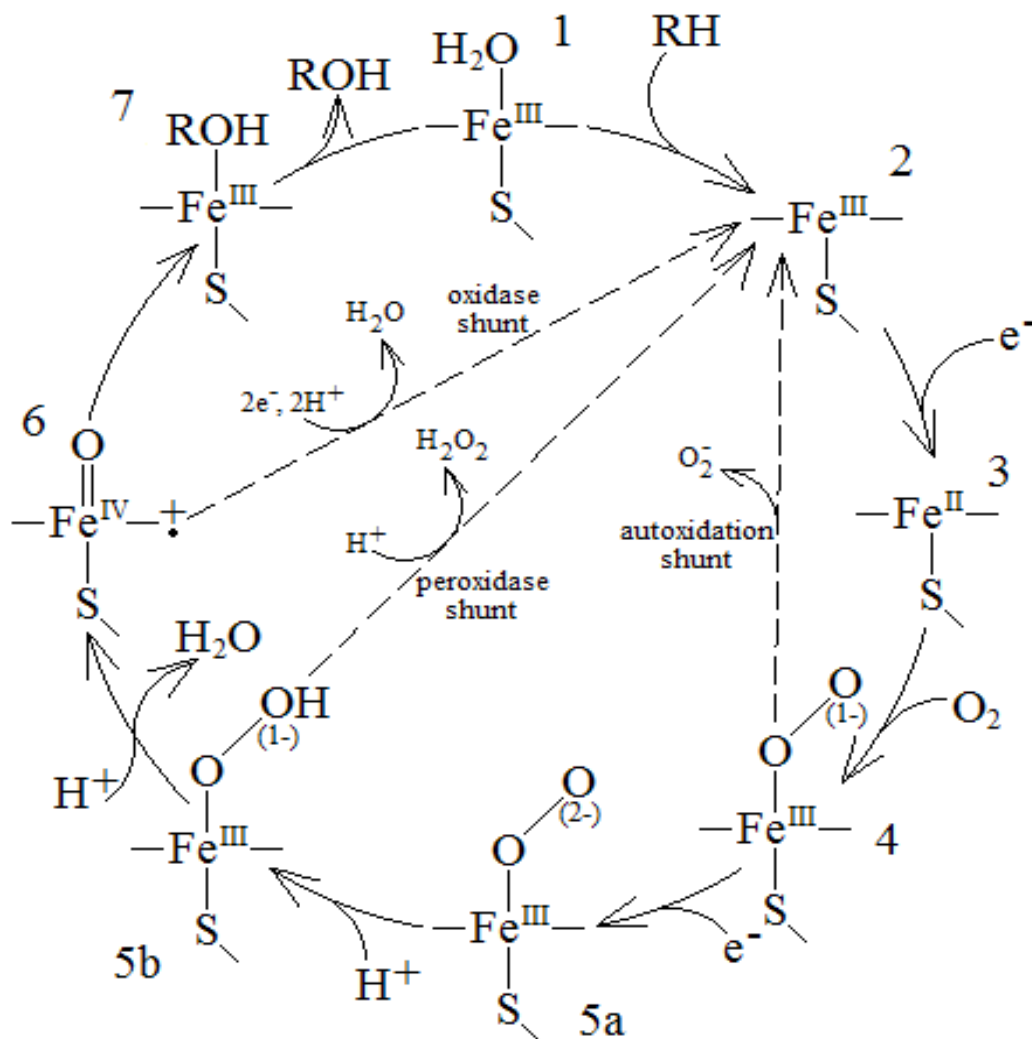
Figure 1 – Reaction cycle of CYP. R-H represents substrate. Adapted from Denisov et al., 2005.

1.2 Cytochrome P450 2C9 (CYP2C9)

CYP2C9 is clinically the most important member of CYP2C subfamily and even though it shares more than 82% of amino acid identity with three other human members CYP2C8, CYP2C18 and CYP2C19, their substrate specificity differ significantly (Miners and Birkett, 1998). It was found that 10% to 20% of commonly prescribed drugs (more than 100) are substrates of CYP2C9. It metabolizes many clinically important drugs including the diabetic agent tolbutamide, the anticonvulsant phenytoin, the *S*-enantiomer of the anticoagulant warfarin, Δ1-tetrahydrocannabinol and numerous anti-inflammatory drugs such as ibuprofen, diclofenac, piroxicam, tenoxicam, mefenamic acid, the antihypertensive losartan, and several new drugs including the antidiabetic drug glipizide and the diuretic torasemide (Anzenbacher and Anzenbacherová, 2001; Goldstein, 2001)

1.2.1 Polymorphism and CYP2C9 Allele Frequencies

There are currently 35 identified allelic variants of CYP2C9 (see Table 1), though only two variants different to the typical allelic variant CYP2C9*1 with clinical consequences. The respective allele frequencies for the CYP2C9*1, CYP2C9*2 and CYP2C9*3 variants in Caucasian populations have been reported to range from 0.79–0.86, 0.08–0.125, and 0.03–0.085 (Miners and Birkett, 1998). In African population frequencies of these CYP2C9*2 and CYP2C9*3 alleles are only 4% and 2% respectively, and only CYP2C9*3 out of these two is known in Asian population with frequency approximately 3%. On the other hand two other alleles CYP2C9*11 with frequency 2.7% and CYP2C9*5 with frequency 1.8% found in African population are very rare in both Asian and Caucassian patients (Kirchheiner and Brockmöller, 2005).

Table 1 – CYP2C9 alleles known to date according to The Human Cytochrome P450 (*CYP*) Allele Nomenclature Database (Sim and Ingleman-Sundberg, 2010, http://www.cypalleles.ki.se) downloaded from web on 5/2/2011.

Allele	Effect	Allele	Effect	Allele	Effect
*1 (wt)	none	*13	L90P	*25	118Frameshift
*2	R144C	*14	R125H	*26	T130R
*3	I359L	*15	S162X	*27	R150L
*4	I359T	*16	T299A	*28	Q214L
*5	D360E	*17	P382S	*29	P279T
*6	273Frameshift	*18	I359L, D397A	*30	A477T
*7	L19I	*19	Q454H	*31	I327T
*8	R150H	*20	G70R	*32	V490F
*9	H251R	*21	P30L	*33	R132Q
*10	E272G	*22	N41D	*34	R335Q
*11	R335W	*23	V76M	*35	R125L, R144C
*12	P489S	*24	E354K		

CYP2C9*2 variant shows *in vitro* that maximal reaction rate V_{max} is reduced by 50% while Michaelis constant K_m remains almost unchanged resulting in only minor reduction of activity of patients with heterozygous CYP2C9*1/*2 genotype and moderate reduction of activity of patients with homozygous CYP2C9*2/*2 genotype. On the other hand, the activity of CYP2C9*3 variant is dramatically reduced by both increased K_m and reduced V_{max}, resulting in moderate reduction of activity of patients with heterozygous CYP2C9*1/*3 genotype and very low activity of patients with homozygous CYP2C9*3/*3 genotype (Kirchheiner and Brockmöller, 2005). The major effect of *5 variant is increase of K_m (up to 12-fold higher for hydroxylation of (S)-warfarin) resulting in similar decrease of activity as of *3 variant carriers (Dickmann et al., 2001). *11 variant exhibits increased

both K_m and less significantly even V_{max} resulting in moderately reduced activity during *in vitro* studies (Blaisdell et al., 2004).

1.2.2 Crystal Structures of CYP2C9

There are three crystal structures of CYP2C9 known up to date. First two of them 1OG2 and 1OG5 (Williams et al., 2003) were prepared in resolution 2.60 Å respectively 2.55 Å. CYP2C9 construct prepared for crystallization contained seven amino acid substitutions in the area of F/G loop and F- and F'-helices: K206E, I215V, C216Y, S220P, P221A, I223L and I224L. Also N-terminal transmembrane anchor (residues 1 to 29) was removed and C-terminal end was extended by four histidine tag for easier purification by affinity chromatography. 1OG5 is crystallized with ligand (S)-warfarin bound in the cavity near to the active site, while 1OG2 is crystallized without any ligand.

1R9O crystal structure was prepared at 2.0 Å resolution with ligand flurbiprofen bound in the active site cavity. This construct was prepared the same C-terminal four histidine tag and N-terminal anchor (residues 1 to 22) was replaced by MAKKT sequence derived from modified N-terminus of rabbit CYP2C5 optimized for expression and crystallization. No other mutations were used to modify catalytic domain, which allowed crystallization of structure in its native structure, but also forbid to define several residues from electron density maps. These include residues 26, 38-42, 214-220 (F/G loop) and residues on both ends (Wester et al., 2004).

1.2.3 Structural Features of CYP2C9

CYP2C9 is composed from two domains: catalytic and transmembrane. Catalytic domain is composed from 12 main right-handed α-helices (labeled by letters from A to L according to their position in primary structure), loops with labels of two adjacent helices, 3 β-sheets labeled with numbers (see Figure 2) and heme c cofactor composed from iron atom coordinated with porphyrin, with 2 propionate, 2 vinyl and 4 methyl substituents (see Figure 3, Williams et al., 2003).
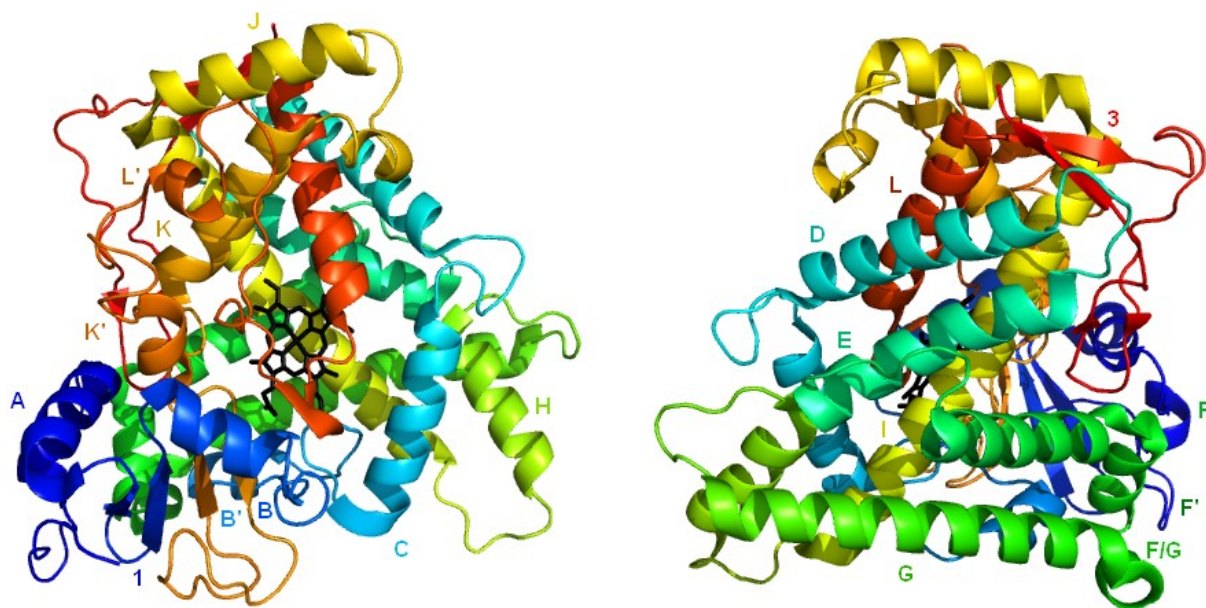
Figure 2 – Catalytic domain of CYP2C9 construct 1OG2 (Williams et al., 2003) with named secondary structures. Heme is shown in black.
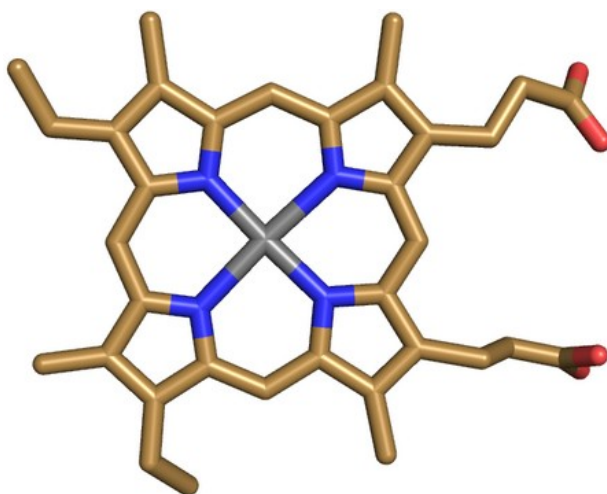
Figure 3 – Stick model of heme c from 1OG2 structure (Williams et al., 2003). For atom types consult Color Chart at page 50.

Crystal structure 1OG2 shows water molecule hydrogen bonded to Thr301 that serves as the proton-transfer path. Heme iron atom is pentacoordinated to Cys435 sulfur atom (see Figure 4). Heme is also stabilized by hydrogen bonds between carboxylic groups of heme propionates and side chains of Arg97, Trp120, Arg124, His368 and Arg433. Arg97 is also fixed in position by hydrogen bonds with carbonyl oxygens of Val113 and Pro367 (see Figure 5, Williams et al., 2003).

Figure 4 – Bond between heme iron and Cys435 and water molecule hydrogen bonded to Thr301 in the active site of 1OG2 construct.
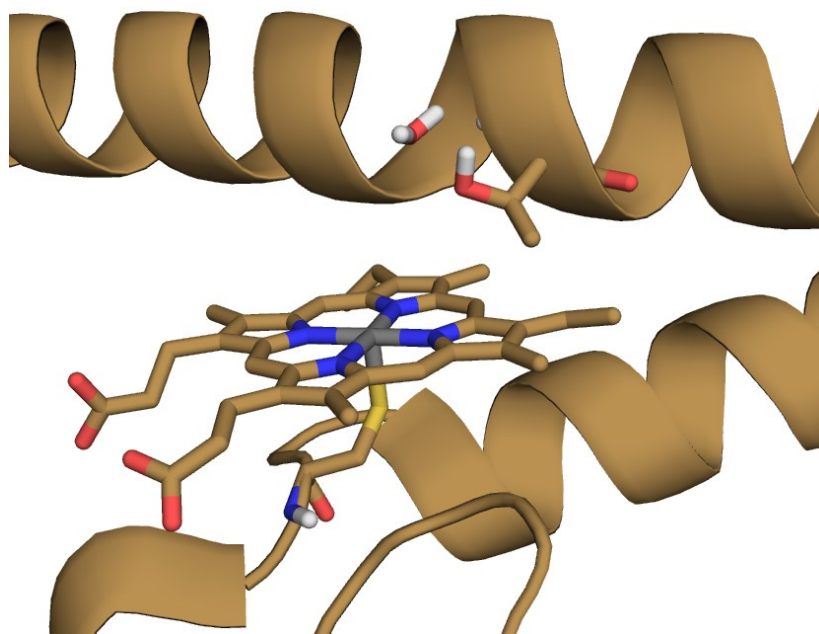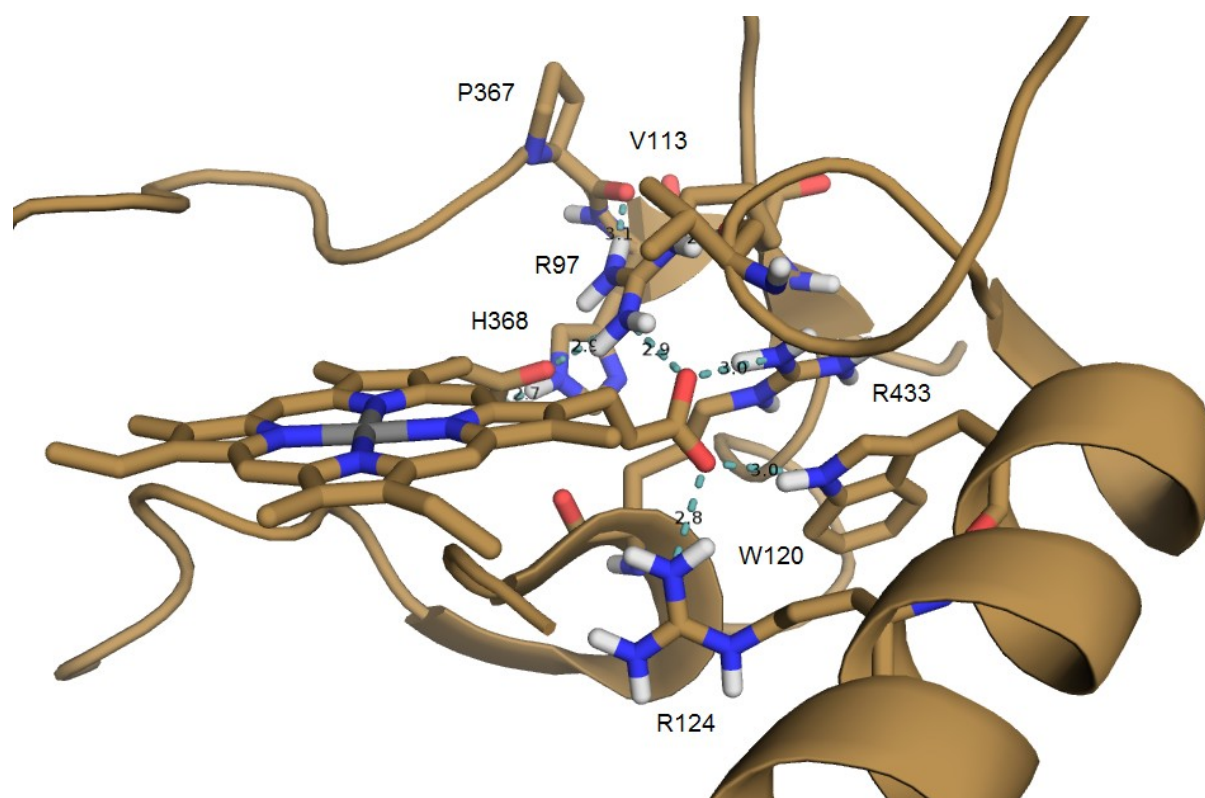

Figure 5 – Heme and residues previously experimentally identified as forming hydrogen bonds with heme propionates with measured distances in Å as blue dotted lines in 1OG2 construct.

1.2.4 Substrates of CYP2C9

CYP2C9 substrates are usually weak acids with aromatic cycle that have the anionic group in distance of approximately 7 Å from hydroxylated carbon atom (Miners and Birkett, 1998). From pharmaceutical drugs we could mention groups of vitamin K antagonists acenocoumarol, phenprocoumon and warfarin, nonsteroidal anti-inflamatory drugs (NSAIDs) like celecoxib, diclofenac, flurbiprofen, lornoxicam, piroxicam and many more, antidiabetic drugs like glyburide and tolbutamide, or angiotensis I receptor antagonist losartan (Kirchheiner and Brockmöller, 2005).

1.2.4.1 Warfarin

Warfarin is anticoagulant drug prescribed mainly in North America and Asia (Kirchheiner and Brockmöller, 2005). It is secondary metabolite of plant Sweet-clover (*Melilotus officinalis)*. It was originally used as rat poison, causing death by internal bleeding in rodent (Wardrop and Keeling, 2008), threatening warfarin-treated human patients with reduced warfarin clearance as well (Kirchheiner and Brockmöller, 2005). While activity of CYP2C9 towards (R)-enantiomer of warfarin is almost zero (Haining et al., 1999), more potent (S)-warfarin from approximately 80% to 85% undergoes CYP2C9 catalyzed biotransformation mostly to 6- and 7-hydroxy (S)-warfarin in 1:3 ratio (Miners and Birkett, 1998). It was found that not only activity but also stereospecifity of enzyme can be heavily influenced by mutations in the active site of enzyme, as mutants of phenylalanines 100, 114 and 476 show have also 4'- and 8-hydroxylase activity towards (S)-warfarin (Mosher et al., 2008) and even towards (R)-warfarin (Haining et al., 1999; see Figure 6).
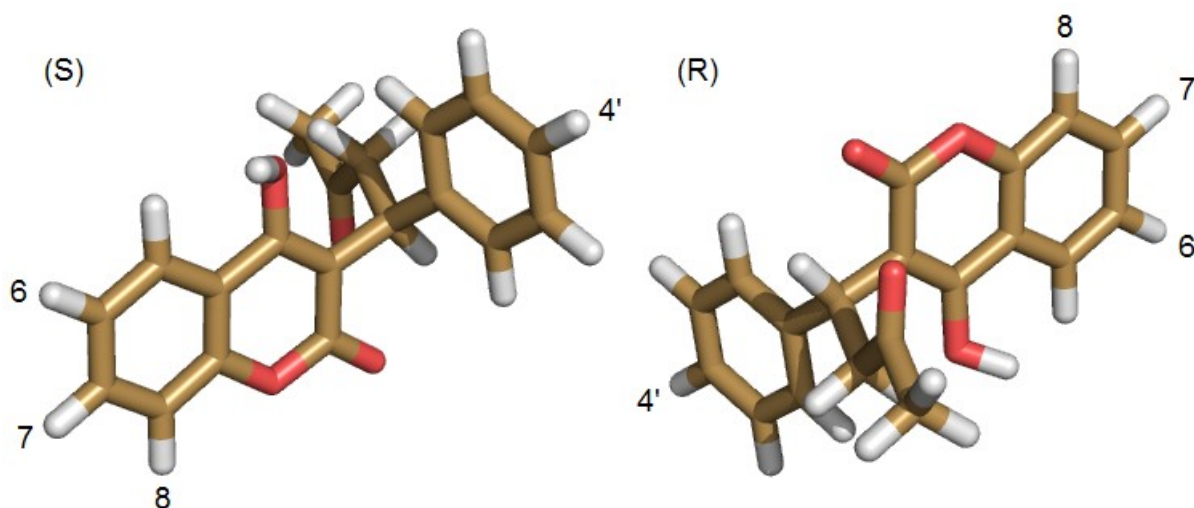

Figure 6 – (S)- and (R)- enantiomers of warfarin with numbered sites of catalytic hydroxylation. Structures downloaded from NCBI BioSystems Database PubChem Compound (Geer et al., 2010, http://www.ncbi.nlm.nih.gov/pccompound).

1.2.4.2 (S)-flurbiprofen

(S)-flurbiprofen is another NSAID which is metabolized by CYP2C9 to product 4'-hydroxyflurbiprofen (Tracy et al., 2002; see Figure 7). Its adverse effects include gastritis, analgesic, nephropathy, fluid retention and allergic skin reaction (Kirchheiner and Brockmöller, 2005).

Figure 7 – The structure of (S)-flurbiprofen with marked 4'- site of hydroxylation. Structure downloaded from NCBI BioSystems Database PubChem Compound (Geer et al., 2010, http://www.ncbi.nlm.nih.gov/pccompound).

1.2.4.3 Diclofenac

Diclofenac is used for its antibacterial properties as nonsteroidal anti-inflamatory drug (NSAID). Its mechanism of action is inhibition of enzyme cyclooxygenase (COX) leading to inhibition of synthesis of lipidic compounds prostaglandins (Dastidar et al., 2000). Typical dose-related adverse effects of diclofenac are gastritis, acute gastric bleeding, renal effects and allergic skin reaction (Kirchheiner and Brockmöller, 2005). In the first step of its metabolism it is hydroxylated in 4' position by CYP2C9 (Dickmann et al., 2004; see Figure 8).
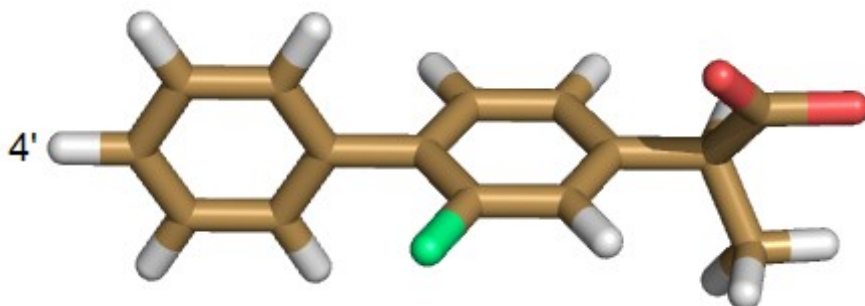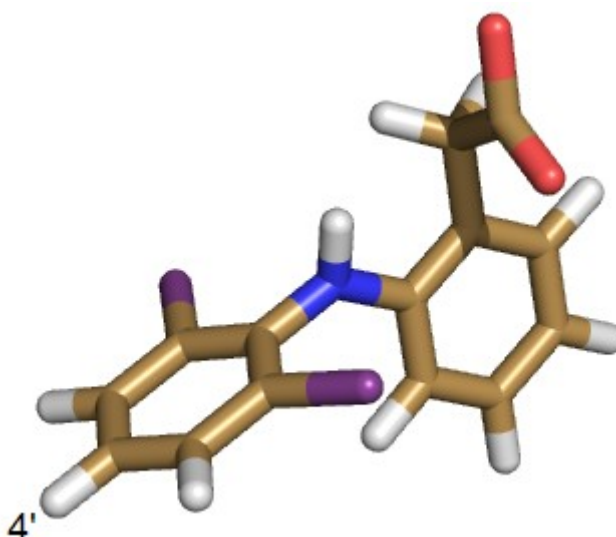

Figure 8 – The structure of diclofenac with marked 4'- site of hydroxylation. Structure downloaded from NCBI BioSystems Database PubChem Compound (Geer et al., 2010, http://www.ncbi.nlm.nih.gov/pccompound).

2 Experimental Methods

2.1 Molecular Dynamics

Molecular dynamics (MD) simulations are used to simulate the behaviour of molecules from single small ligands to large biomacromolecules or systems like phospholipid bilayers in the environment under defined conditions (usually physiological) – temperature, pressure or salinity. Processes and attributes such as flexibility, stability or opening and closing of channels and cavities in time can be investigated by MD. They can be also used to evaluate *in silico* prepared or modified molecules and to predict their conformational changes (van Gunsteren and Mark, 1998; Nezbeda et al., 2002).

2.1.1 Basics of Molecular Dynamics Simulations

MD simulations are based on classical mechanics' principles, describing motion of system composed of N interacting atoms by Newton's equations of motion, that is solved simultaneously for all atoms in differential time steps (typically femtoseconds) repeatedly over some timespan (typically nanoseconds):

$$m_i \frac{\partial^2 \boldsymbol{r}_i}{\partial t^2} \; = \; \boldsymbol{F}_i, \; i \; = \; 1 \dots N \,. \tag{1}$$

Forces are then computed as negative derivatives of potential function V defined by force-field and by atomic positions:

$$\boldsymbol{F}_i \; = \; -\frac{\partial V}{\partial \boldsymbol{r}_i} \tag{2}$$

The trajectory of simulation system is a result of computed coordinates as a function of time. It is usually observed that after a period of initial changes, the system reaches equilibrium state and averaged structures from this part can be used to evaluate macroscopic properties of system. However, errors in parametrization of force-field can lead to artificial behavior (Ditzler et al, 2010).

Some approximations are used by MD algorithm to ensure real-time availability of results:

➢ all electrons are in their ground states, because force is computed as function of atom coordinates only,

➢ force fields providing forces are approximate and user-modifiable,

➢ force field is pair additive,

➢ long range Lennard-Jones and sometimes even long-range Coulomb interaction are cut-off at some defined distance,

➢ periodic boundary conditions are used to avoid unwanted boundary of border particles with vacuum (Hess et al., 2012a).

2.1.2 Energy Minimization

The potential energy function of system forms very complex landscape with one global minimum and many local minima. They are connected by saddle points. Unfortunately, there is currently no method able of quick and easy finding of global minimum in real time. Therefore GROMACS uses the steepest descent energy minimization method using information about potential derivative to move step by step in the direction of negative gradient towards the nearest local minimum. Size of single step influences speed of search, but cannot be set up too high to ensure that motion is always downhill (Hess et al., 2012b).

2.1.3 Analysis of MD Results

2.1.3.1 Ramachandran Plot

Protein backbone is composed from series of rigid planar peptide groups. Its conformation can be specified by dihedral angles φ [phi] (around Cα-N bond) and ψ [psi] (around Cα-C bond). Values of these angles are defined as 180° for all-trans conformation. Ramachandran plot is 2D visualisation of their distribution for every amino acid in protein with value of angle φ marked on horizontal axis and value of angle ψ marked on vertical axis. Only some conformations are sterically allowed and therefore the surface of plot can be divided between the allowable areas and restricted areas with border regions between them. Shape and size of these regions is different for every amino acid (see Figure 9). Ramachandran plot is usually used for validation of stereochemistry of both crystal and *in silico* prepared structures (Voet and Voetová, 1995).
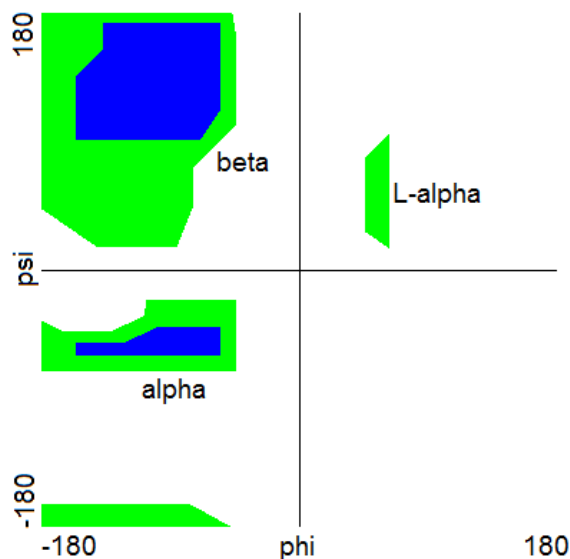

Figure 9 – Ramachandran plot with computed allowable areas (blue color) and generously allowed areas (colored with green) for poly-L-alanine peptide corresponding with marked secondary structures beta sheet (beta), right handed alpha helix (alpha) and left handed alpha helix (L-alpha). Created in VMD (Humphrey et al., 1996, http://www.ks.uiuc.edu/Research/vmd/) using Ramaplot plugin.

2.1.3.2 Root Mean Square Deviation (RMSD)

RMSD is a measure of average distance of certain atoms in protein with respect to a reference structure. The structure (t_l) is least-square fitted to a reference structure ($t_2 = 0$) first and then RMSD is calculated according to formula:

$$RMSD(t_1,\ t_2)\ =\ [\frac{1}{M}\sum_{i=1}^{N}m_i\|\boldsymbol{r_i}(t_1) - \boldsymbol{r_i}(t_2)\|^2]^{\frac{1}{2}}\ , \tag{3}$$

where $\boldsymbol{r}_i$ (t) is position vector of certain atom i at time t.

Calculation of RMSD is used during fitting where one structure is translated and rotated over another structure in order to minimize RMSD, as well as for evaluation of the course of trajectory where is RMSD calculated between every steps (Coutsias et al., 2004; Hess et al., 2012c).

2.1.3.3 Atomic Root Mean Square Fluctuation (RMSF)

RMSF describing flexibility of amino acids is used to evaluate changes in rigidity and flexibility of secondary structures of mutants compared to wild-type variant. Relation of crystallographic Debye-Waller temperature factors also known as B-factors is described by formula:

$$B_f\ =\ \frac{8\pi^2}{3}RMSF^2\ , \tag{4}$$

where B_f means B-factor.

Results of MD studies are generally similar to X-ray data, although because of the structural relaxation occurring over the course of MD simulation, some parts of structure exhibits increment or decrement of flexibility. On the other hand, due to low frequency with which is the conformation space sampled, simple MD run itself doesn't suffice to provide full description of protein flexibility occurring during passage of substrates and products through channels (Otyepka et al., 2012).

2.1.3.4 Volumes

Volumes of the active cavity was measured with use of CASTp server (http://sts-fw.bioengr.uic.edu/castp/calculation.php; Dundas et al., 2006) from snapshots from MD simulations with deleted water molecules, included HET atoms of heme and probe radius 2.0 Å.

2.2 Docking

Docking is a computational procedure for prediction how small molecules, such as substrates or drug candidates, bind to a receptor of known 3D structure. Desired results are binding affinity, described by free energy, and the bound conformation. This method is especially important in drug design and studies of unavailable structures.

There are few premises made by this method:

➢ receptor is completely or mostly rigid structure,

➢ charges of receptor atoms do not change during binding.

To evaluate noncovalent bonds by free energy (the lower the energy is, structures will bind in given conformation more likely) program uses scoring function describing standard chemical potentials of the system, based on physical models of van der Waals interactions and electrostatic Coulombic forces (similarly as in MD force fields) and empirical information from databases.

Scoring function can be described as:

$$c = \sum_{i<j} f_{t_i t_j}(r_{ij}) \quad , \tag{5}$$

where f is interaction function of atom types t_i and t_j in distance r; it is a summation over all atom pairs separated by up to 3 covalent bonds and is composed of both intraatomic and interatomic contributions.

There is variety of optimization method of docking algorithm from local procedures like calculating gradient of scoring function in addition to its value, to algorithms like simulated annealing, particle swarm optimization or genetic algorithms (Trott and Olson, 2010).

Extreme reduction of time cost of process is achieved by pre-calculation of different grid map for each atom type of docked ligand. It is three dimensional lattice of points evaluating interactions of certain atom with the environment of user defined region of interest, usually active site of enzyme. Distances of grid points varies from 0.2Å to 1.0Å. Each grid point is followed by probe calculating total energy over all atoms of protein with all pairwise interactions and within a non-bonded cut off radius, according to parameters of each ligand atom type (Morris et al., 1998).

3 Materials and Methods

3.1 Structure

CYP2C9 crystal structure PDBID 1OG2 (Williams et al., 2003) was used as a template for structure preparation. Chain B and waters were removed from original PDB file downloaded from RCSB Protein Data Bank (Bernstein et al., 1977, http://www.rcsb.org/pdb) in Pymol 1.4rc program (Schrödinger, 2011, http://www.pymol.org). Wild type form of CYP2C9 was reestablished from chain A using Mutagenesis Wizard with rescue mutations E206K, V215I, Y216C, P220S, A221P, L222I and L223I (for details, see Figure 10). Incomplete His491 residue at C-terminal was removed. Structures of all studied mutants were created from this structure with same procedure.
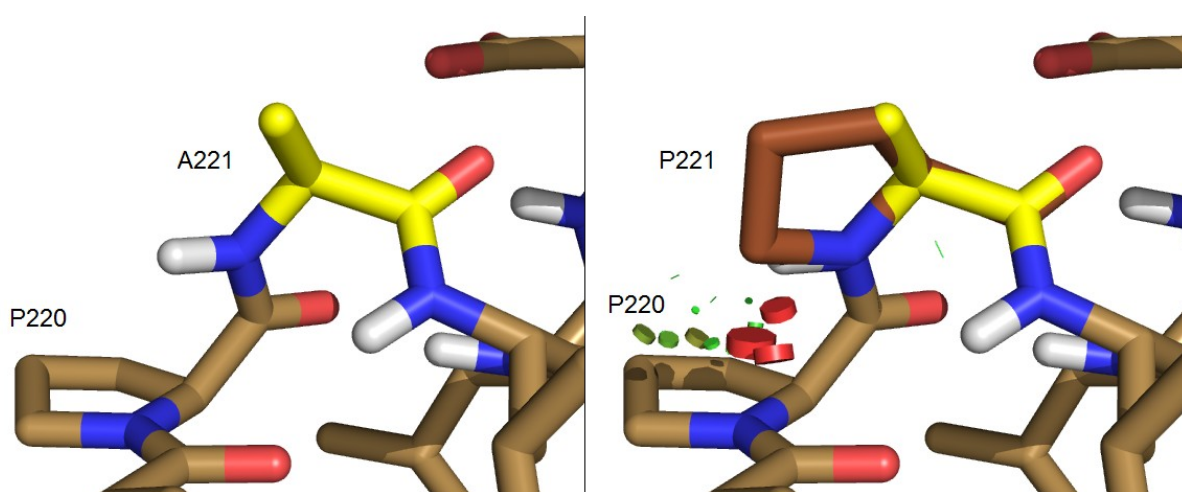

Figure 10 – Example of *in silico* mutagenesis. Selected residue highlited on left panel was selected in Mutagenesis Wizard in Pymol. Several orientations were considered and the one with the most favourable contacts (shown in green) and the least nonfavourable contacts (shown in olive and red) with surrounding residues was selected (right panel).

3.2 Molecular Dynamics

Molecular dynamics simulations was performed with Gromacs 4.5.1 with GROMOS96 53a6 force field (Oostenbrink et al., 2004). Starting system for MD simulations was box with 1 cytochrome. Original box was extended to 7.1 x 6.3 x 7.8 nm and it was filled with SPC/E extended simple point charge water molecules (Berendsen et al., 1987) and NaCl with concentration 0.150 mol/L. Since heme should be covalently bound to Cys 435 in the CYP2C9 structure, we have added parameters for the covalent bond between heme Fe and cysteine sulphur (see Table 2).

Table 2 - Parameters defining attachment of heme to C435. All distances and angles were measured from CYP2C9 crystal structure and they were symmetrized, force constant parametrized according to comparison of similar bonding found in GROMOS 53a6 force field (Oostenbrink et al., 2004).

Atoms	Parametres
S_{cys}-Fe_{heme}	2.3 Å, $0.500 \cdot 10^6$ kJ·mol^{-1}·nm^{-1}
C_{cys}-S_{cys}-Fe_{heme}	115°, 50.0 kJ·mol^{-1}·rad^{-2}
S_{cys}-Fe_{heme}-N_{heme}	90°, 320.0 kJ·mol^{-1}·rad^{-2}
N_{heme}-Fe_{heme}-N_{heme}	180°, 420.0 kJ·mol^{-1}·rad^{-2}

Molecular dynamics (MD) simulations of each mutant structure were started firstly with energy minimization in 1500 steps by steepest-descent algorithm with initial stepsize 0.01 nm and maximum converged force 1000 kJ/mol·nm. Second, all heavy atoms (CONS) were positionally restrained for 1-ns long MD pre-run. Finally, 100-ns long free production MD runs were performed. Snapshot structures were created for docking and analysis of trajectories after each 10 ns. Energy minimization of each snapshot has no visible effect on snapshot structure quality according to Ramachandran plots created in VMD (Humphrey et al., 1996, http://www.ks.uiuc.edu/Research/vmd/) using Ramaplot plugin (see Figure 12 in Results section) and therefore energy minimization of each snapshot was omitted.

3.3 Substrate Docking

3D structures of CYP2C9 substrates diclofenac, S-flurbiprofen, S-warfarin and R-warfarin were downloaded from NCBI BioSystems Database PubChem Compound (Geer et al., 2010, http://www.ncbi.nlm.nih.gov/pccompound). Their carboxyl groups were deprotonated in PyMOL. AutoDock Tools program suite from MGLTools 1.5.6 RC2 (Sanner, 1999, http://mgltools.scripps.edu/) was used to prepare ligands by an addition of Gasteiger charges, merging of non-polar hydrogens, detection of aromatic carbons and setting up the torsion tree. Docking was performed with AutoDock Vina (Trott a Olson, 2010, http://vina.scripps.edu/) with structures of CYP2C9 mutants generated by molecular dynamics every 10 ns. Grid for docking procedure was 40 Angstrom long in each direction and active site was detected as a cavity above heme moiety. Iron on the heme moiety was set to +1 or +2 formal charge, however such change did not changed results of docking significantly. Default Vina parameters were used for the docking procedure itself.

4 Results

4.1 Mutants of CYP2C9 – Literature Review

Based on data from databases SuperCYP (Preissner et al., 2010, http://bioinformatics.charite.de/supercyp) and The Human Cytochrome P450 (*CYP*) Allele Nomenclature Database (Sim and Ingleman-Sundberg, 2010, http://www.cypalleles.ki.se) was prepared compendium of previously measured activities of CYP2C9 mutants compared to activities of wild-type variant. (Appendix A)

Unfortunately, only relatively old studies from late 90's are available about (R)-warfarin and they provide drastically different results. Some consider 4'-OH-(R)-warfarin to be main product of hydroxylation by wt and I359L with V_{lim} about twice of that of (S)-warfarin hydroxylation but with value of K_m 2 or 3 orders higher (Sullivan et al., 1996). Other reports only very low activity towards its 6- and 7-hydroxylation by both these variants (I359L 5-fold lower than wt), with about half of their activity towards its 8-hydroxylation only by wt (Haining et al., 1996), with much higher activity of F114L mutant with 4':6:7:8 ratio about 3:1:1:0.3 (Haining et al., 1999). Also reported increment of V_{lim} of (S)-warfarin 7-hydroxylation by I359L (Sullivan et al., 1996) is contradictive to newer findings (Dickmann et al., 2001). Therefore we do not know for sure what is main product of hydroxylation of (R)-warfarin and we do not possess any valuable kinetic parameters of this reaction.

4.2 *in silico* Mutagenesis

Due to the literature review, we have prepared wild-type several mutant variants of CYP2C9 (see Table 3 and Figure 11). **I359L** mutant (*3 allele) has greatest clinical consequences from all known CYP2C9 mutations due to both: significantly reduced CYP2C9 activity even of heterozygous carriers with most pharmaceutical drugs and high frequency in African and White populations (Kirchheiner and Brockmöller, 2005). Mutations of residues **Phe114** and **Phe476** in the active site were previously extensively studied and it was shown, that they are responsible for stereospecificity of warfarin enantiomers hydroxylation, as well as for usually lower activity towards other substrates (Mosher et al., 2008). **Arg97** is determinant of catalytic function as charged residue in the active site, but its exact function remains unknown (Ridderström et al., 2000). Also due to the fact that previous study experienced great difficulties during expression and purification of R97F mutant *in vitro* (Dickmann et al., 2004).

Table 3 – Performed mutations and their known kinetic parameters in format V_{lim}/K_m, or activity (in *italics*) where only results of single activity essay are available, compared to wt (Dickmann et al., 2001; Guo et al., 2005; Haining et al., 1996; Haining et al., 1999; Mosher et al., 2008; Tracy et al., 2002).

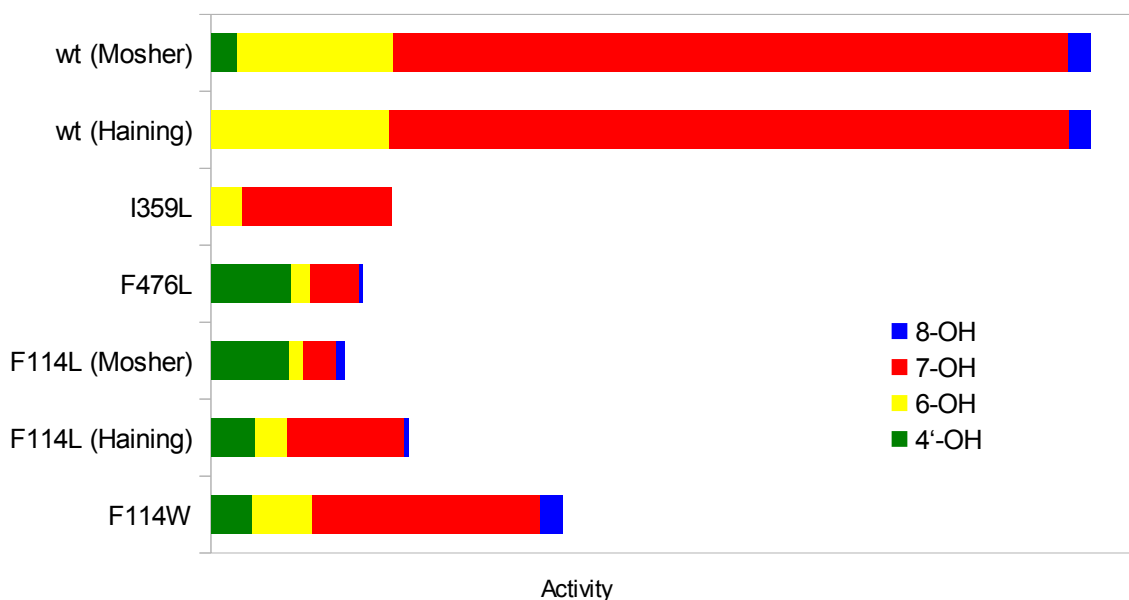| $\dfrac{V_{lim}}{K_m}$	I359L	F476L	F114L	F114W
(S)-warfarin	lower higher	lower higher	lower higher	lower lower
(R)-warfarin	*lower*		*higher*	
(S)-flurbiprofen	lower higher	lower higher	disputed higher	unchanged unchanged
diclofenac	lower or unchanged higher	*unchanged*	unchanged higher	*higher*

Figure 11 – Regiospecifity of (S)-warfarin hydroxylation (Haining et al., 1996; Haining et al., 1999; Mosher et al., 2008).

4.3 Molecular Dynamics Simulations

4.3.1 Structure Validation

We have generated both energy minimized and non-energy minimized snapshots after each 10 ns from produced trajectories and analyzed them using Ramachandran plots. It was found that Ramachandran plots of trajectory snapshots used for docking show values of dihedral angles Phi and Psi inside their allowable and generously allowed regions, therefore structures are useful, and also that there are no significant differences between Ramachandran plots of snapshots before and after their energy minimization (see Figure 12).
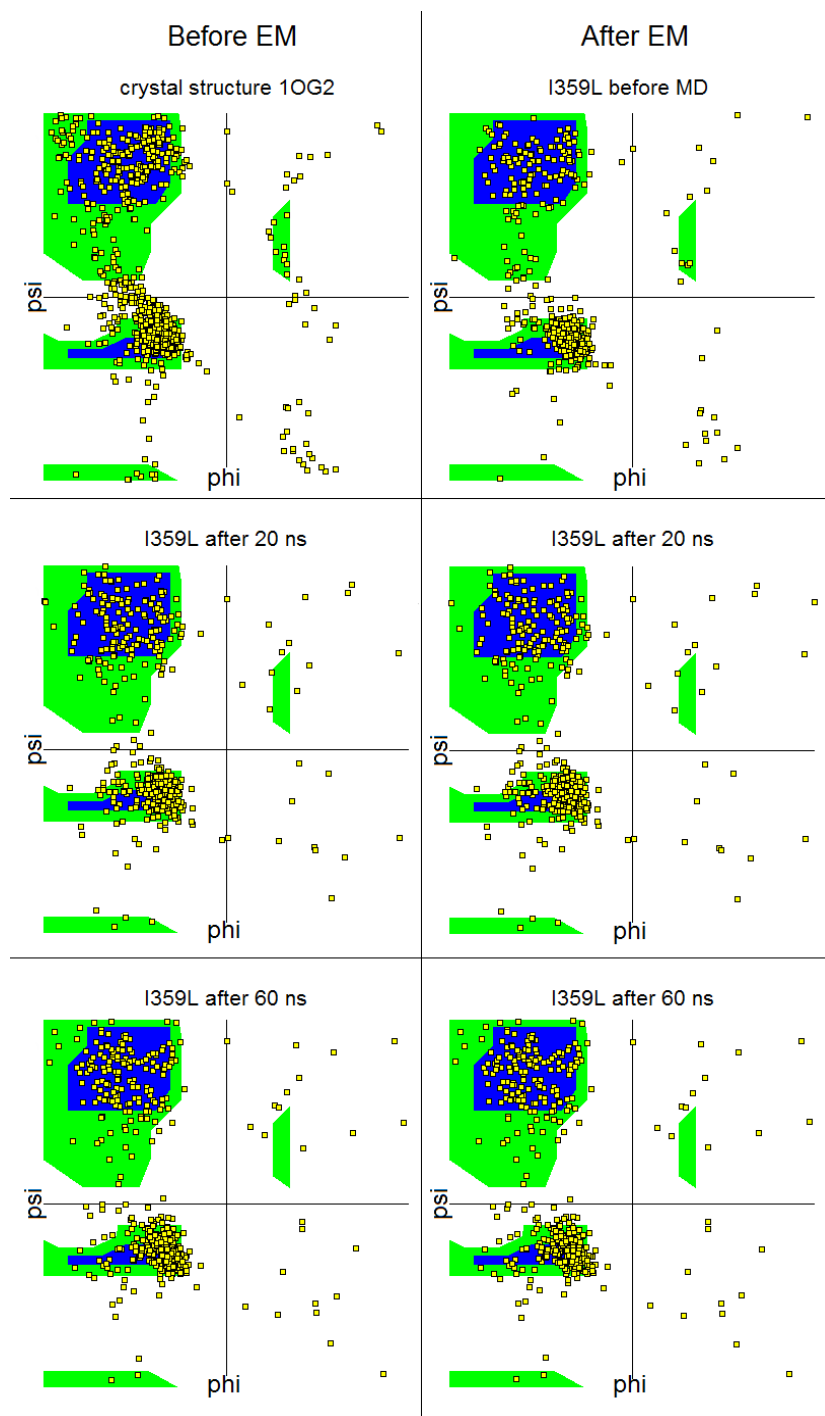

Figure 12 – Ramachandran plots of CYP2C9 mutants before and after energy minimization.

4.3.2 Trajectory Analysis

Snapshots after each 10 ns were produced from 100 ns long MD runs. For sample trajectory of CYP2C9 F114W mutant see Figure 13.
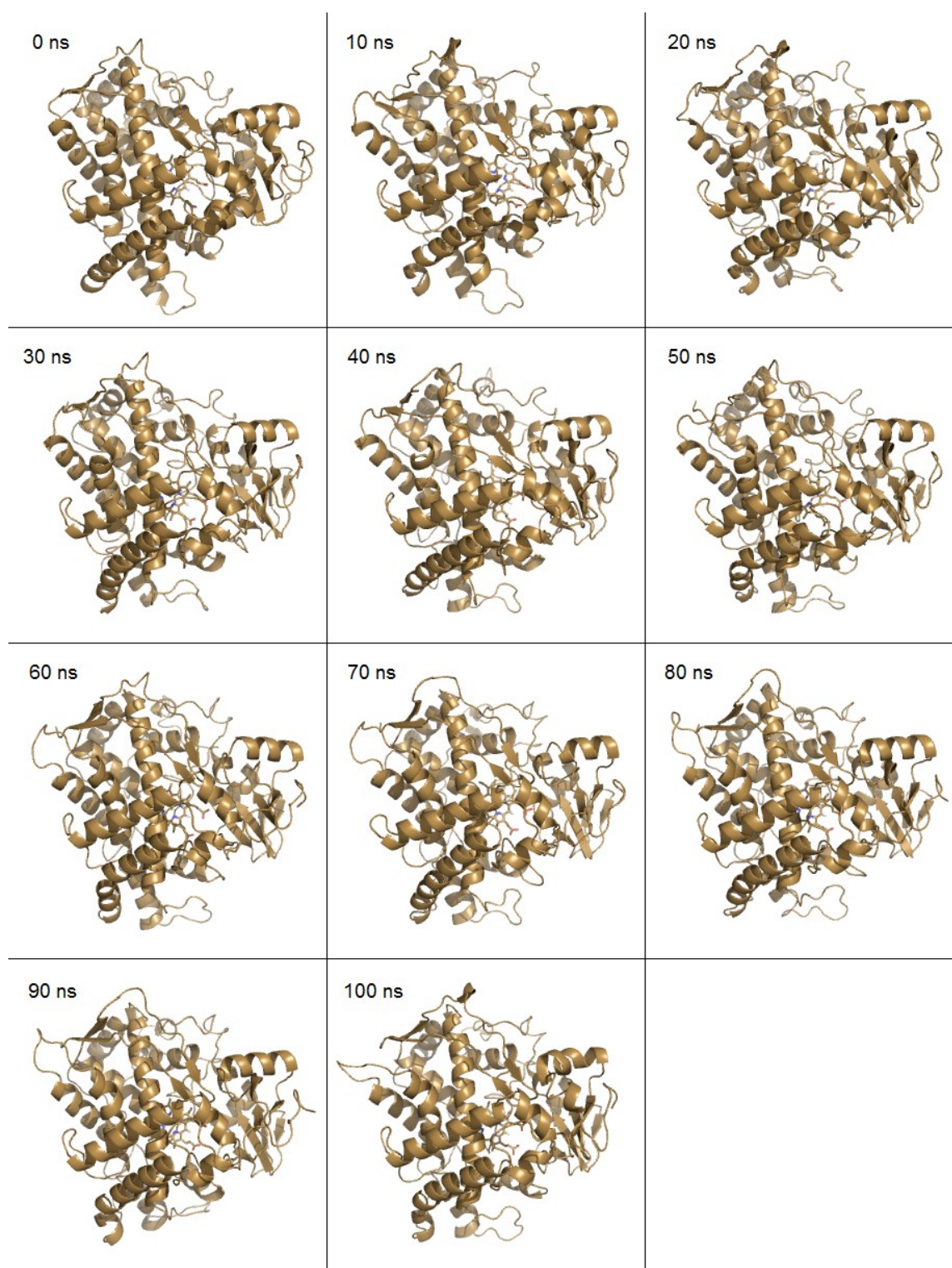

Figure 13 − 10 ns snapshots obtained from 100 ns long MD run of F114W mutant.

4.3.2.1 RMSD

Root mean square deviations of alpha carbons and heme atoms of all produced trajectories were calculated with time step 100 ps. The average RMSD values were similar for all structures ranging from 0.27 to 0.32 (see Table 4). From RMSD time evolution, it is apparent (see Figure 14) that all structures reach equilibrium state mainly during first 20 ns and mostly show no further significant structural changes over the longer run.

Table 4 – Average RMSD values from 100 ns long MD runs of studied structures.

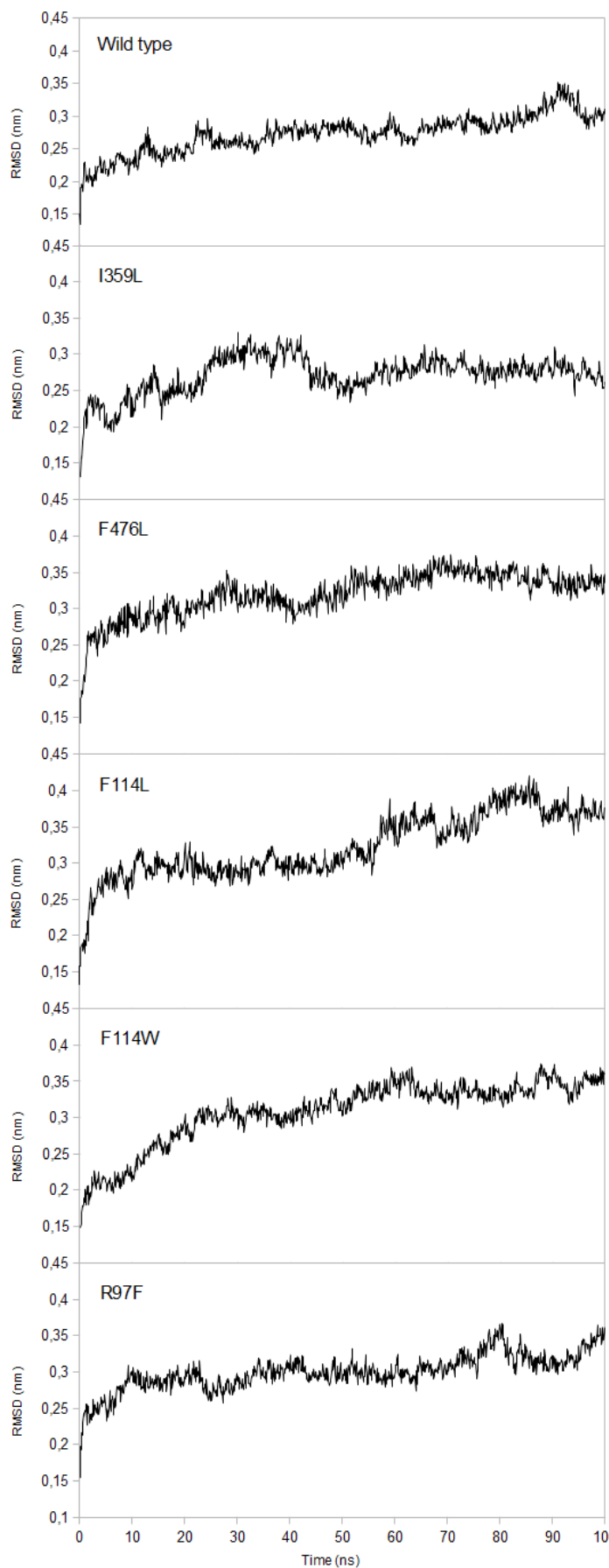| Structure	Average RMSD (nm)
wt	0.27 ± 0.03
I359L	0.27 ± 0.03
F476L	0.32 ± 0.03
F114L	0.32 ± 0.04
F114W	0.31 ± 0.04
R97F	0.30 ± 0.03

Figure 14 – RMSD plots of studied structures during 100 ns long MD run.

4.3.2.2 Flexibility

To compare flexibility of prepared structures, RMSF of each residue was calculated from average structure from last 5 ns of 100 ns long MD runs.

Results show, that the most rigid parts of **wildtype** structure are I-, K-, L- and E-helices, while the most flexible parts are A-, C- and J-helices and 2 sheet (see Figures 15 and 16). The highest peak with value of 0.4269 nm is at Asn277 that is part of H/I loop.

I359L mutant has significantly reduced flexibility of F/G, G/H and H/I loops and B-helix, while increased flexibility was found at F-helix and D/E and K/L loops and C-terminal loop near to the area of mutation (see Figures 15 and 16).

Flexibility of **F476L** mutant is highly reduced in the area of introduced mutation, on C/D, F/G, G/H and H/I loops, on B-, B'- and E-helices and on 2 sheet. Increased flexibility was observed only on K/L loop and slightly on J-helix (see Figures 15 and 16).

F114L mutant compared to wt exhibits high increment of flexibility at 3-3 and 3-2 sheet and the loop between them, as well as at D- and G- helices, as compensation of flexibility decrement in the surroundings of active site (and mutation), mostly that of B-, C- and F'-helices and F/G loop, and small decrement shows even I-helix (see Figures 15 and 16).

Flexibility of **F114W** mutant is significantly increased in the area of D/E loop, followed by K/L loop, L-, A- and E-helices. Decreased flexibility was observed at B/B', G/H and H/I loops (see Figures 15 and 16).

R97F mutant exhibits highly increased flexibility towards both ends of chain: mostly at A-, K- and K'-helix and K/L loop, while the mutation site, B-, E-, F-, F'- and I-helices, B/B', F/G and G/H loops and 1-1, 1-2 and 2 sheets are more rigid than in wt variant (see Figures 15 and 16).
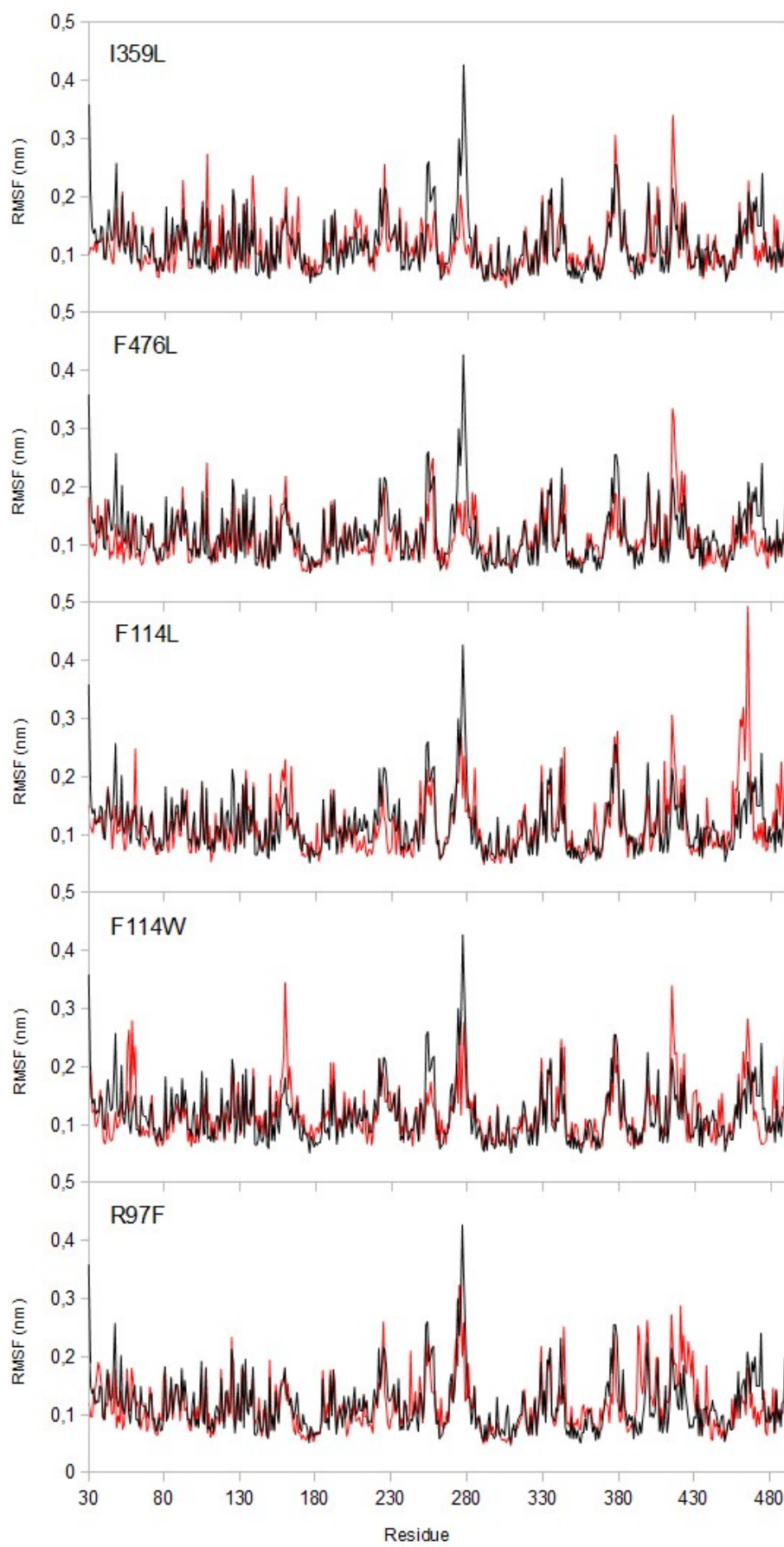
Figure 15 – RMSF of studied mutants (in red) compared to wt (in black) calculated from average structure from last 5 ns of the trajectory.
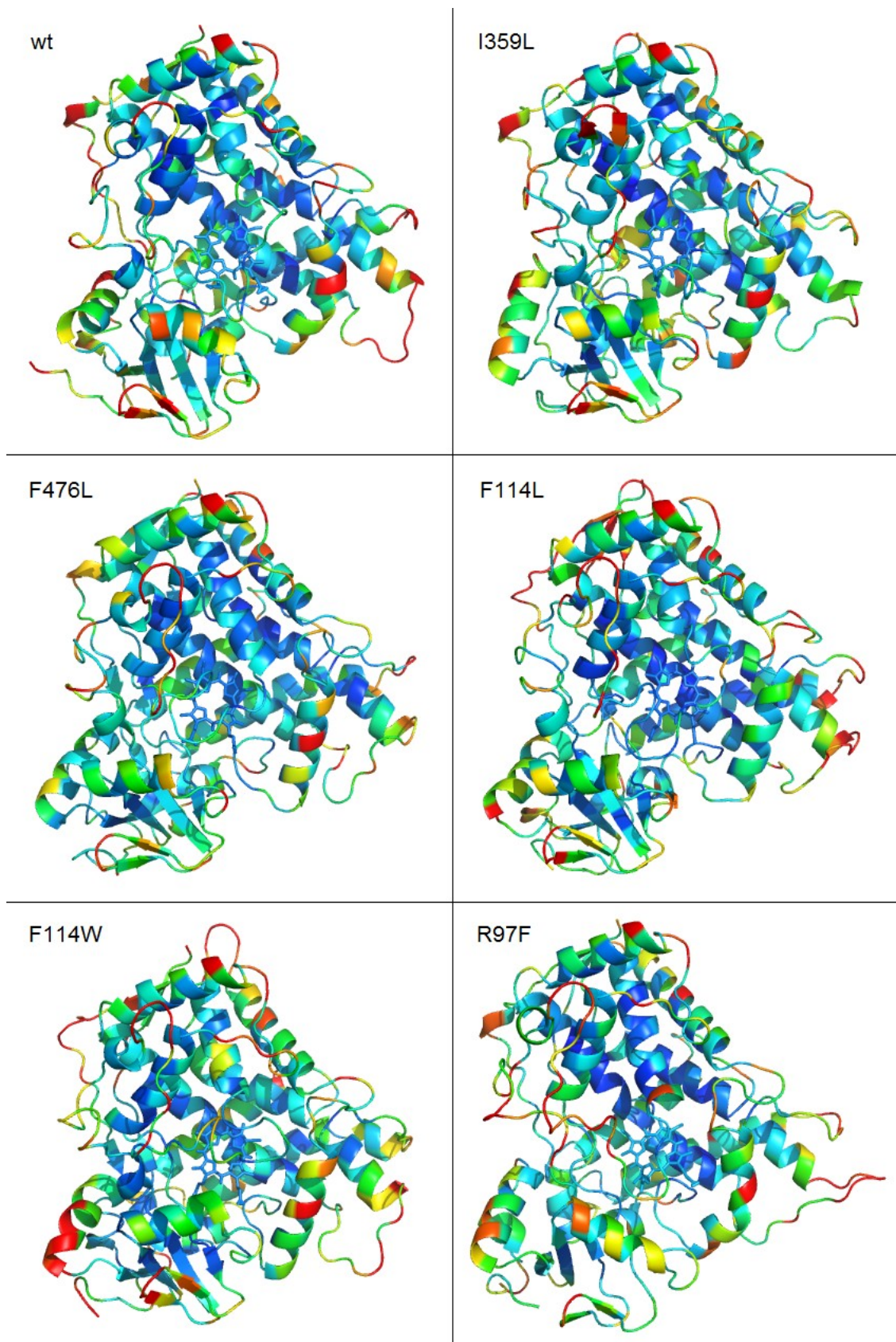
Figure 16 – Flexibility of studied structures calculated from average structure from last 5 ns of the trajectory and depicted as color from dark blue for the most rigid parts to red for the most flexible parts.

4.3.2.3 Structural changes

Secondary structure of **wild type** variant remains stable during the course of 100 ns trajectory. with the exception of temporary formation of very short (only a few AAs long) helices or sheets at some of highly flexible loops located at the peripheries of the enzyme. (see Table 5).

Table 5 – Observed secondary structure of CYP 2C9 wildtype variant.

SS	Residues	SS	Residues	SS	Residues
A'-helix	45-45	E'-helix	172-182	2-1 sheet	374-376
A-helix	50-61	F-helix	192-208	2-2 sheet	379-381
1-1 sheet	64-69	F'-helix	211-218	1-3 sheet	384-390
1-2 sheet	75-77	G-helix	232-253	K'-helix	392-395
B-helix	80-89	H-helix	263-273	L'-helix	409-412
B'-helix	101-106	I-helix	284-315	L-helix	443-455
C-helix	117-130	J-helix	318-331	3-3 sheet	457-460
D-helix	141-158	K-helix	346-358	3-2 sheet	485-488
E-helix	166-169	1-4 sheet	368-370		

Tertiary structure of **wild type** is from the beginning almost the same as that of original crystal structure, the most notable and significant change is straightening of the end of L/L' loop beneath the heme. The only part of enzyme that seems unstabilized at the end of trajectory is F'-helix with F/F' loop that are still moving being pushed by B'-helix.

Active site cavity is pretty large (1,360 $Å^3$) and shaped like mushroom standing on top of the heme. At 10 ns snapshot, heme is moved a little towards its propionates compared to original crystal structure and slowly moves to its original position during the simulation as it slides slightly under I-helix reducing cavity volume and reaches its final position (still 0.8 Å further from I-helix than originally) after 60 ns and remains stable thereafter. This movement seems to be caused by repulsion between L/L' loop and B'-helix, that later results in movement of B-helix towards heme (around 70 ns) followed by gradual bending of B'/C loop into cavity, which seems to reach new stable conformation after 80 ns (see Figure 17 (a)). In 90 ns snapshot is cavity almost closed by side chains of Phe114, Glu300, Leu361 and Leu362, and while contribution of Phe114 located on misplaced B'/C loop is undoubted, the enclosure seems to be caused mainly by random orientation of other three named residues, as cavity opens again in 100 ns while Phe114 remains at the same position, even though its overall volume is still significantly reduced (710 $Å^3$).

Both Phe114 and Phe476 are located on cavity surface. Ile359 is located on loop after K-helix

but is not at the cavity surface itself. At the beginning of trajectory Arg97 forms H-bonds with only Val113 and heme propionate at the side of Pro367 (right propionate) while left propionate is bent away from its reach. After 30 ns left propionate straightens back to the level of heme and hydrogen bonds to Arg97 while right propionate bends away under the heme, where it stays till the end of the simulation.

I359L mutant has the same stable secondary structure as wt, but its tertiary structure differs slightly as the C-terminal loop moves slightly into cavity after 60 ns and remains stable in its new position. End of L/L' loop under the propionates bends away from heme in the very beginning in contrast to wt and heme remains at the same position as in original crystal structure (see Figure 17 (b)).

Volume of active site cavity is reduced (1,120 Å^3) in all snapshots most notably in its bottom part. This is caused by loop containing studied I359L mutation. Even though its overall shape remains unchanged, side chain of Leu359 is directed towards long C-terminal loop and I-helix and probably this repulsion pushes Leu361 and more importantly Leu362 about 2 Å into cavity (see Figure 17 (c)). These residues with their surroundings also have increased flexibility in I359L mutant.

F476L mutant contain slight shifts from wt in the secondary structure of A-helix, I-helix and L-helix, whereas the most notable changes in tertiary structure are bending of I-helix into the cavity, also bending of G-helix and translation of A- and F-helices. Also B'-helix changes its position repeatedly during trajectory, but important part of B'/C loop including Phe114 remains unaffected. The end of L/L' loop is rather deformed and squeezed under the heme.

Active site cavity size is reduced (1,100 Å^3) especially in its lower part by overlap of heme by I-helix, though this overlap is much smaller than in case of F114 mutants. Glu300 also sticks deeper into the cavity due to bent I-helix. While Leu361 is at the same position as in wt, Leu362 and especially Pro363 and Thr364 are moved higher above heme and also deeper into the cavity (see Figure 17 (d)). Also Leu208, Leu476 and Ala477 are much higher above heme, while residues at B/B' loop are pushed little closer towards heme center.

F114L mutants' most significant structural changes are bending of I-helix into the active site cavity, greatly reducing its volume (700 Å^3). Loop after K-helix differs significantly from wt, especially in the second half of trajectory, Leu361 and Leu362 are much lower than in wt while Pro363, Thr364, Ser365 and Leu366 are moved significantly higher above heme and also deeper into the cavity (see Figure 17 (e)). B'-helix and the first part of B'/C loop up to Phe110 moves more into cavity while its remaining part (containing studied mutation) moves only a little lower. Leu114 has same side chain orientation to the cavity as Phe114 in first half of wt trajectory.

F114W mutant differs from wt with orientation of 2 sheets and B-, B'- a G-helices. L/L' loop is deformed under the heme so that it do not reach B-helix. Heme position is stable and same as in the crystal structure. This mutant shows similar behavior to F114L structure with equivalent consequence – decreased active site cavity volume (920 $Å^3$). However, the cavity is bigger that in F114L especially in first half of trajectory (1,070 $Å^3$) because Arg97 is significantly moved to the side forming hydrogen bonds only with Val113 and left heme propionate leaving free space in between heme propionates. Also compared to wt the transition between lower part of cavity (which resembles "mushroom's leg") and its upper part ("mushroom's head") is much less apparent resulting in its overall shape resembling flattened ball, that allows relatively easy access of heme iron.

Trp114 is located slightly higher above heme than Phe114 in wt and further reduces cavity volume due to its greater size. Furthermore it changes side chain orientation notably in the middle of trajectory. While in the first half of simulation is plain of its cycles approximately parallel to original Phe114 in wt, in the second half it rotates into vertical orientation. Part of loop after K-helix near heme is significantly repositioned. While Asp360 and Pro367 remain at same positions as in wt, Leu361 and Leu362 are positioned much lower and their side chains are directed underneath the heme. On the other hand, Thr364 and Pro363 are moved into the cavity above heme (see Figure 17 (f)).

R97F mutant shows unstable tertiary structure. While the side chain of Phe97 was initially directed towards the heme in the same manner as Arg97 in wt variant, it turns to the opposite direction within the first 20 ns of simulation, while B/B' loop remains at the same position. Heme propionates later bent away from the cavity but their hydrogen bonds to remaining residues are similar to that in wt until 70 ns, when heme starts to lean and slides away from cavity also reducing its volume. At this point, the tertiary structure starts to melt and B-, C- and L-helices start to move away from heme's path, while the heme moves (see Figure 17 (g)).
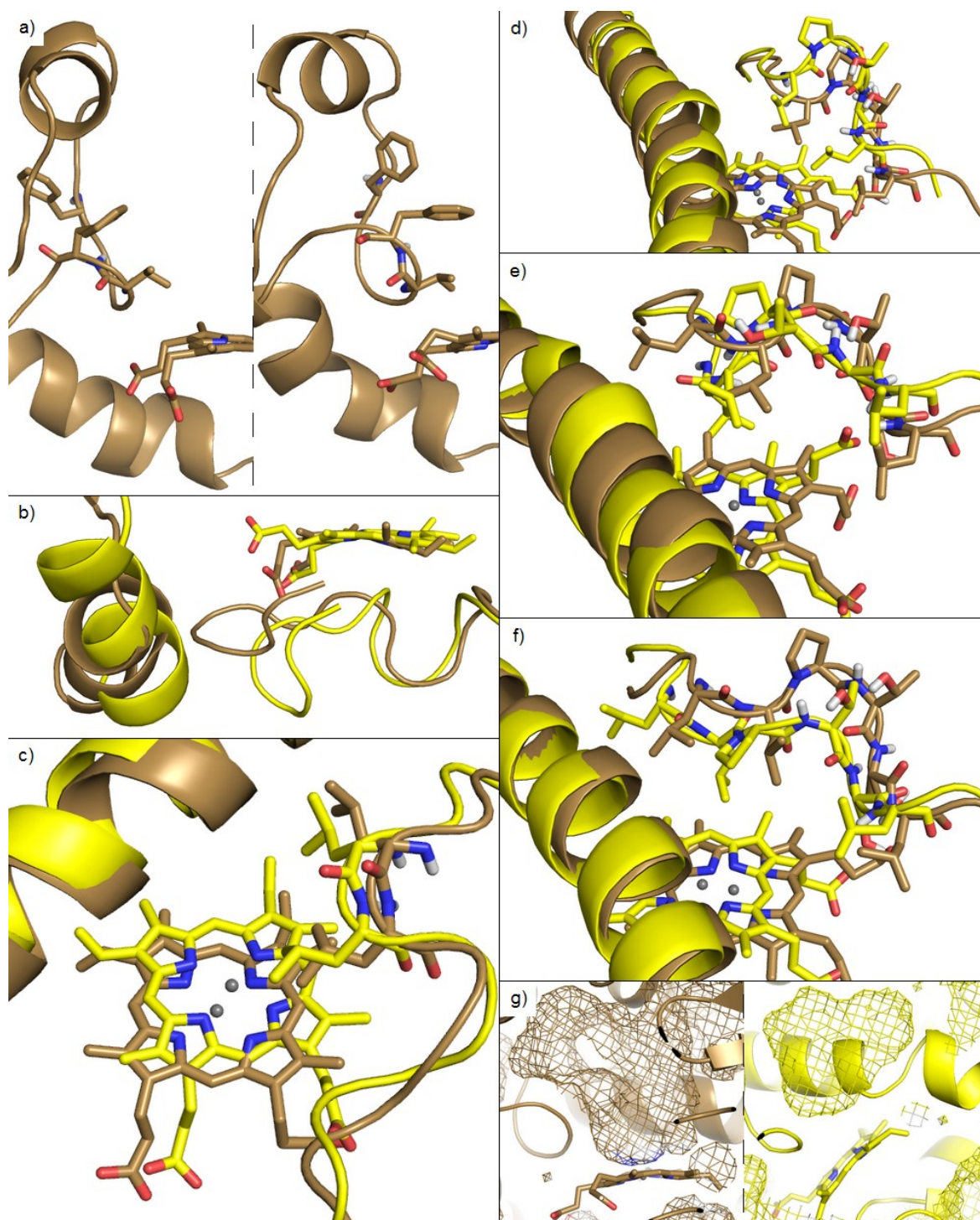
Figure 17 – The most significant structural changes of CYP2C9 variants from MD simulations.
(a) Positions of B'/C loop in **wt** in 60 ns (left panel) and 100 ns (right panel), L110, V113 and L114 shown as stick figures. **(b)** L/L' loop and B-helix of wt and **I359L** at 60 ns (mutant structures are always highlighted with yellow). **(c)** Position of I-helix and loop after K-helix of wt and **I359L** at 60 ns, L361 (on the top) and L362 are shown as stick figures. **(d)** Position of I-helix and loop after K-helix of wt and **F476L** at 60 ns, L362 (on the left), P363, T364, S365 and L366 are shown as stick figures. **(e)** Position of I-helix and loop after K-helix of wt and **F114L** at 60 ns, L361, L362, P363, T364, S365 and L366 are shown as stick figures. **(f)** Position of I-helix and loop after K-helix of wt and **F114W** at 40 ns, L361, L362, P363, T364, S365 and L366 are shown as stick figures. **(g)** Heme and active site cavity of wt and **R97F** at 100 ns.

4.4 Docking

Docking of each ligand has been evaluated according to (i) the distance between heme iron and site-of-metabolism, (ii) for number of effective positions between 20 most energetically favorable poses for each structure (see Table 6 for their overall comparison) and (iii) for presence of particular residues interacting with ligand. Affinities measured by docking program Vina could not have been used as they did not showed any significant differences. Number of acquired efficient docking positions differed greatly between every ligand, with the most "active" poses present for both warfarin enantiomers and the least "active" poses for diclofenac.

While (S)-flurbiprofen usually accesses heme from only a few specific positions due to its shape (long and narrow), all the others studied ligands share bent L-shape and their tails can adopt various positions while they are bonded to heme iron. Therefore each ligand binds in a slightly different conformation.

Table 6 – Comparison of ligand docking in format "frequency of efficient structures" / "distance from heme iron" compared with wt, based only on stable parts of trajectories.

	I359L	F476L	F114L	F114W
(S)-warfarin	lower higher	lower higher	lower higher	higher higher
(R)-warfarin	lower higher		lower higher	
(S)-flurbiprofen	higher higher	higher higher	higher higher	higher unchanged
diclofenac	higher higher	unchanged higher	unchanged higher	higher higher

4.4.1 Wild type

Docking into wt structure was generally similar between individual frames with two peaks of activity around 30 and 70 ns and with zero activity of 90 ns snapshot.

(S)-warfarin can access heme either with coumarin or phenyl ring. First position is present during whole trajectory with distance between iron and closest carbon from 2.9 to 4.0 Å in closest positions. The most often the closest atom is C-7 followed by C-6, and in some cases also C-8. Positions docking by phenyl were on the other hand acquired in lower quantities and similar distances, but only after the first 30 ns of trajectory.

In the first case, coumarin ring interacts with Leu362, Leu366, Val113 and Ala297 that are located just above the heme. Other residues creating hydrophobic interactions with the rest of molecule are from the most to the least important Leu208, Phe114, Phe476 and Ile205. π-stacking has been observed in about one third of efficient positions between Phe476 and ligand's phenyl ring. Hydrogen bonds were present in about half cases mostly with Glu300, followed by Ser209 and sometimes also Thr364 (see Figure 18 (a)).

In the second case, phenyl ring interacts with Leu361, Leu362, Leu366, Ala297 and only sometimes with Val113, that on the other hand hydrophobically bonds to the rest of ligand's molecule together with Leu208 and Phe476. Hydrogen bonds are also present, but not very frequently, usually with Glu300, Ser209, Thr364.

(R)-warfarin has its nearest carbons 3.4 to 4.0 Å from heme iron in its best positions. Closest carbon of its coumarin is slightly more often C-6 than C-7. Positions with phenyl ring near the heme are missing in first two snapshots (10 and 20 ns). Also in docking into 100 ns snapshot there were no positions closer to heme iron than 5 Å and structures approaching heme by phenyl ring were more numerous than those approaching by coumarin side.

In structures with coumarin ring near the heme, it interacts with Leu362, Leu366, Val113, Ala297. Rest of ligand binds hydrophobically to Leu208 and often to Phe476, Ile205 and Phe114. π-stacking is quite rare in larger part of trajectory. Hydrogen bonds are present quite often mostly with Glu300, Ser209 or Thr364.

In structures with phenyl ring near the heme, it interacts with Leu362, Leu366, Val113, Ala297. Rest of ligand binds hydrophobically to Leu208, Phe114, Phe476. Hydrogen bonds are present quite often mostly with Glu300, Ser209 or Thr364 (see Figure 18 (b)).

(S)-flurbiprofen docks well only in some structures spread through trajectory, most notably at 50 and 80 ns with distances 3.6 to 4.0 Å. It forms aliphatic interactions between terminal phenyl ring and Leu362, Leu366, Val113 and Ala297, while its terminal methyl bonds to Phe476, Phe114. Middle phenyl usually binds with the same aliphatic residues from both sides with addition of Leu361. It also forms π-stacks usually with Phe114. Fluorine atom forms almost no hydrogen bonds, while carboxyl group makes them often, but to various residues or peptide bond nitrogens (see Figure 18 (c)).

Diclofenac docks well at 20 or 30 ns with best distances around 3.5 Å, but in the rest of trajectory only at 60 and 80 ns with distances above 5 Å. It interacts mostly between its terminal phenyl ring and Leu362 with Leu366. Its middle phenyl ring interacts mostly with Phe476 and also with Leu362 and Leu366. Only carboxyl group makes any hydrogen bonds but quite nonspecifically with various residues (see Figure 18 (d)).

4.4.2 I359L

While we have received many docking efficient positions at the beginning of trajectory, their number dropped rapidly towards zero at 30 ns snapshot for all ligands. It then slowly increased towards maximum at 80 ns snapshot, where almost all positions seemed to be catalyticaly efficient. Types of interactions and interacting residues do not differ from those in wt, but shortest distances from heme iron are for all ligands higher, from 4.2 Å in case of (S)-flurbiprofen and diclofenac to 4.4 Å for (R)-warfarin and 4.7 Å for (S)-warfarin (see Figure 18 (e) and (f)).

4.4.3 F476L

While we have received many docking efficient positions at the beginning of trajectory, especially at 20 ns, their number dropped rapidly immediately thereafter and remain stable for the rest of trajectory, with zero activity around 40 and 80 ns for all ligands. Shortest distences between ligands and heme iron vary greatly from 4.3 Å in case of (S)-flurbiprofen, over around 5.5 Å for diclofenac and (S)-warfarin approaching heme with coumarin to 6.1 Å for (S)-warfarin binding with its phenyl ring. On the other hand interactions with residues remain unchanged and even Leu476 retains function of original residue in hydrophobic binding of ligand (see Figure 18 (g)).

4.4.4 F114L

While in the first 20 ns of trajectory almost nothing docks into F114L mutant snapshots, beginning with 30 ns its docking results become stable, with only slightly higher amount of efficient positions at 70 ns, although less frequent than in wt. Shortest distances from heme iron are prolonged to 4.6 Å for (S)-flurbiprofen, 4.7 Å for both warfarin enantiomers and 5.6 Å for diclofenac. Interactions with ligands also differ slightly, while Leu114 retains function of original residue in the same manner as Leu476 in F476L mutant, two other residues Val292 and Leu366 newly contribute to hydrophobic binding of ligands and also hydrophobic bonds, especially with Glu300 and Asn107, are formed more often than in wt (see Figure 18 (h) and (i)).

4.4.5 F114W

Docking results of F114W mutant are steady with only slight quantitative maximum around 60 ns. This mutant has greatest number of efficient docking positions of all studied structures for all ligands. Distance of (S)-flurbiprofen is 3.5 Å, which is only 0.1 Å closer than wt, (S)-warfarin approaches heme from 3.7 Å with both its sides, which means it is 0.8 Å farther than coumarin in wt and only 0.4 Å farther than phenyl in wt. Diclofenac docks in distance of 4.2 Å, which is 0.6 Å farther than in wt. This mutant also suffers from greatest changes in interacting residues. While Trp114 retains original function of Phe114 in wt – hydrophobic binding with sporadic π-stacking, it also sometimes forms hydrogen bonds with (S)-warfarin. Leu362 is completely missing and its place is taken by Pro363 (see Figure 18 (j), (k) and (l)).

4.4.6 R97F

Due to apparent decay of R97F mutant heme was not accessible by any ligand in its final form.

Figure 18 ► – Examples of some of the best docking positions on the next page.
(a) Highlighted (S)-warfarin docked by its coumarin into 60 ns snapshot of **wt** in distance of 2.9 Å.
(b) (R)-warfarin docked by its phenyl into 70 ns snapshot of **wt** in distance of 3.3 Å.
(c) (S)-flurbiprofen docked into 50 ns snapshot of **wt** in distance of 3.6 Å.
(d) Diclofenac docked into 30 ns snapshot of **wt** in distance of 3.4 Å.

(e) (S)-warfarin docked by its coumarin into 70 ns snapshot of **I359L** mutant in distance of 4.7 Å.
(f) (S)-flurbiprofen docked into 70 ns snapshot of **I359L** mutant in distance of 4.2 Å.

(g) (S)-warfarin docked by its phenyl into 100 ns snapshot of **F476L** mutant in distance of 6.1 Å.

(h) (S)-warfarin docked by its coumarin into 90 ns snapshot of **F114L** mutant in distance of 4.7 Å.
(i) Diclofenac docked into 90 ns snapshot of **F114L** mutant in distance of 5.6 Å.

(j) (S)-warfarin docked by its coumarin into 40 ns snapshot of **F114W** mutant in distance of 3.7 Å.
(k) (S)-flurbiprofen docked into 40 ns snapshot of **F114W** mutant in distance of 3.5 Å.
(l) Diclofenac docked into 100 ns snapshot of **F114W** mutant in distance of 4.2 Å.
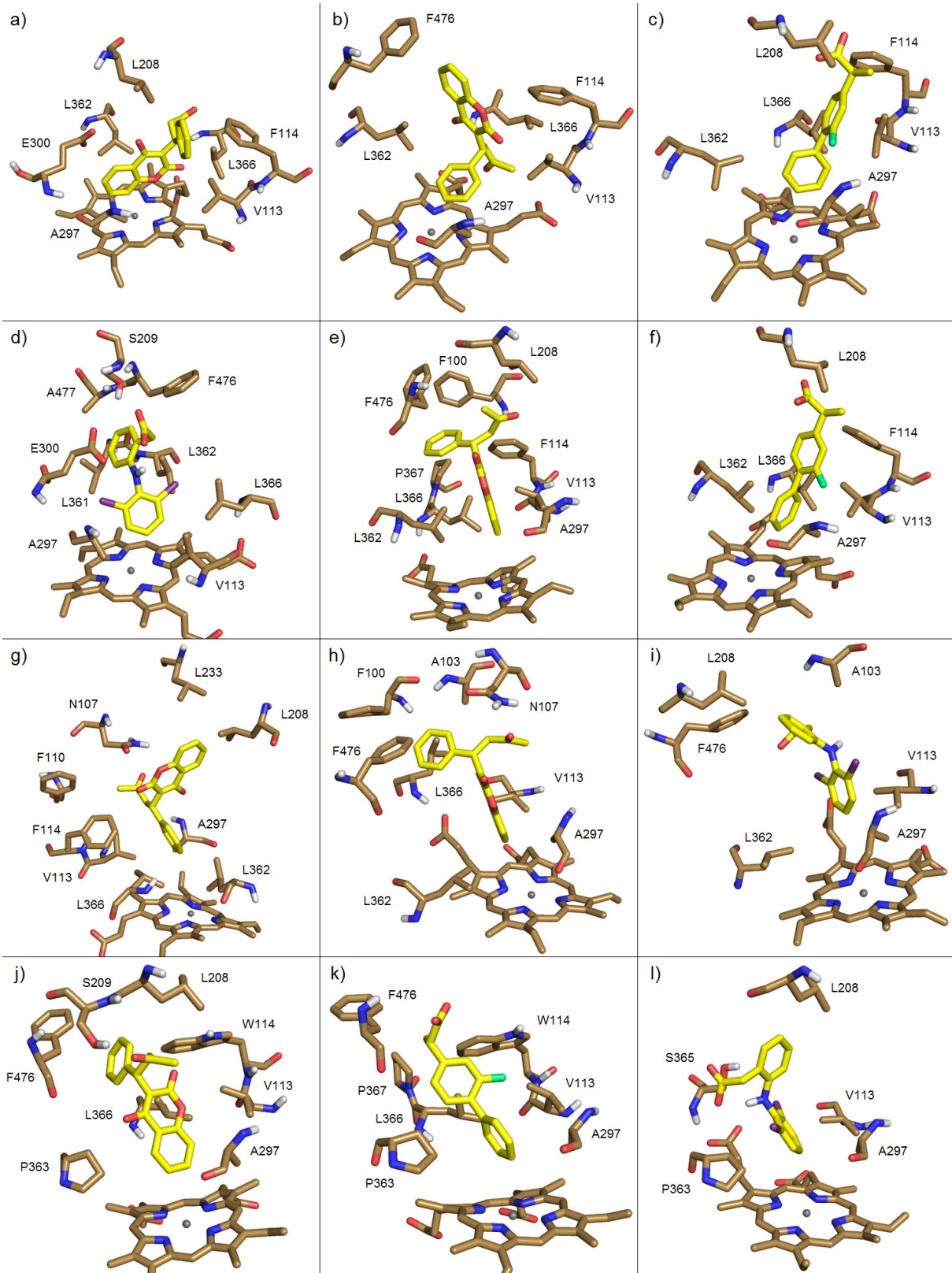
5 Discussion

4'-hydroxy-(S)-flurbiprofen is considered to be the sole product of (S)-flurbiprofen hydroxylation *in vitro* (Miners and Birkett, 1998). Although we have received docking results with both phenyl and methyl groups near heme iron from all studied structures and even though SMARTCyp (Rydberg et al., 2010a; Rydberg et al., 2010b; Rydberg and Olsen, 2012a; Rydberg and Olsen, 2012b; Rydberg et al., 2013a; Rydberg et al., 2013b) considers methyl group the most favorable location of hydroxylation by CYP2C family, the presence of both these positions has already been observed *in vitro* (Hummel et al., 2004). For this reason it seems, that regiospecifity of (S)-flurbiprofen hydroxylation by CYP2C9 has other than steric means, that reach beyond boundaries of this study. Similar situation seems to be with diclofenac 4'-hydroxylation of its final phenyl group while its hydroxylation on 3' and 5 carbons still seems at least theoretically possible (Mosher et al., 2008). Both warfarin enantiomers can approach heme with both coumarin (containing carbons 6, 7 and 8) and phenyl ring (containing carbon 4').

Wild type structure is very similar to that of original crystal (1OG2; Williams et al., 2003). Docking results are similar into the individual frames with small exceptions at 80 ns, when bending of B'/C loop into active site cavity changes its architecture. Driving force for this change could be either repulsion between L/L' loop and B-helix or lesser stability of B'-helix, as its position and shape differs between crystal structures of construct 1OG2 (Williams et al., 2003) used for this study and more native and flexible form 1R9O (Wester et al., 2004).

From interactions between protein and ligands, hydrogen bonding appears to be rather insignificant as it was observed only in minority of catalytically efficient positions with distances 2.9 – 8.0 Å and with various residues as for example Glu300, Ser209, Thr364 or random nitrogens of peptidic bonds. Also π-stacking, that was formerly considered key interaction in substrate binding, was only rarely present (mostly with Phe476, but also with Phe110 or Phe114) even when limitations from rigidity of protein structure were taken into account. On the other hand, hydrophobic interactions were strongly prevalent. Most important aliphatic residues located near the heme interacting mostly with hydroxylated ring of ligand were Leu362, Leu366, Val113 and Ala297. While number of residues interacting with rest of ligands' molecules is greater due to variety of efficient positions, most frequent were hydrophobic interactions with Leu208, Phe114 and Phe476.

Due to the fact that Ile359 does not lie on cavity surface and due to strong analogy between isoleucine and leucine, the lack of structural differences in **I359L mutant** met our anticipation. Docking into its trajectory provided stable results. Most important structural change is transition of Leu361 and Leu362 about 2 Å into cavity reducing volume of lower part of the cavity. While same residues as in wt interact with ligands, best distances from heme iron for all ligands are from

4.2 to 4.9 Å and therefore significantly longer than in wt. This observation seems to be in accordance with reliable *in vitro* studies, as they report drop of activity of this mutant usually due to both decreased value of V_{lim} and increased value of K_m.

The original idea behind preparation of Phe to Leu mutants *in vitro* was assessment of the importance of aromatic interaction with substrate and drop of their activity seemed to confirm this assumption (Mosher et al., 2008). But results of this study show that contribution of aromatic interactions is minimal while these mutations lead mainly to the reduction of active site cavity volume, especially in its part closer to heme, due to deformation of I-helix and loop after K-helix. Both these mutants have reached stable conformation during first 20 ns of their trajectories and their docking results have remained stable ever after.

F476L mutant has middle of I-helix bent over heme with especially Glu300 sticking deep into cavity while at the other side of heme are especially Pro363 and Thr364 repositioned much higher above heme and also close above its middle and Leu366 repositioned up to 4 Å closer to heme. And while these changes do not alter residues interacting with ligands and even Leu476 preserves main function of original residue (hydrophobic binding), distances of ligands from heme iron are most prolonged from all studied mutants. They also vary greatly from 4.3 Å to 6.1 Å. These measurement also seem to correspond with decreased value of V_{lim} and increased value of K_m acquired *in vitro*. Only in case of diclofenac hydroxylation was reported unaltered activity, but unfortunately only results of single activity essay and no kinetic parameters are available (Mosher et al., 2008).

Cavity of **F114L mutant** is altered in similar way by I-helix bending into it as well as loop after K-helix, where Pro363, Thr364, Ser365 and Leu366 are moved up to 5 Å higher above heme compared to wt and towards I-helix, while Leu361 is up to 5 Å lower and its side chain is directed underneath the hem. This structural change seems to slightly alter interaction with ligands. While all hydrophobically interacting residues from wt remain and even Leu114 keeps position and function of original Phe114, there are also two residues newly seen to form aliphatic interactions with ligands: Val292 located on I-helix and Leu366. While there were also no π-stacks present, the amount of hydrogen bonds have risen, mainly due to Glu300 and Asn107. Also increased distances of ligand molecules from heme iron, that were from 4.6 Å to 5.6 Å in best positions, are in accordance with *in vitro* observed increment of K_m.

F114W mutant has stable docking results since the beginning of its trajectory. It exhibits far greatest modification of loop after K-helix. Leu361 and Leu362 are translated lower and their side chains lead underneath heme, while especially Pro363 is repositioned deep into cavity. For this reason Pro363 takes place of Leu362 in forming aliphatic interactions with hydroxylated rings of ligands. Lower part of cavity is especially in the first half of trajectory comparably large with that of wt, it is moved towards right heme propionate due to increased overlap of heme by I-helix (even though it

retains its shape) and due to change of conformation of loop after K-helix together with bending of right propionate (in the first half of trajectory). As upper part of cavity is smaller and Phe476 is located further away from it, Phe476 does not interact with ligands. On the other hand Trp114 retains function of original Phe114 and while it is capable of forming π-stacks, it does so rarely and only interacts hydrophobically with ligands, though it also often forms hydrogen bonds with (S)-warfarin. Distances from heme iron are by far most similar to those of wt in contrast with all other mutants. Unchanged distance of (S)-flurbiprofen is in great accordance with *in vitro* results indicating that both V_{lim} and K_m of this mutant are also unchanged. More complicated is comparison with *in vitro* results for (S)-warfarin, that reports decreased both V_{lim} and K_m. Unfortunately only result available from single activity assay of diclofenac *in vitro* hydroxylation is prohibiting further insight into this problem.

Neither Arg97, nor Phe97 in **R97F mutant** is located on the surface of active site cavity. Arg97 was observed to form backbone for hydrogen bonding of heme propionates in all studied mutants, while Phe97 in this mutant have turned away from heme, that started to lean and slide away from cavity and out from heme at 70 ns. This finding corresponds well with reported problems of heme incorporation and low enzyme stability *in vitro* (Dickmann et al., 2004).

From the comparison between *in vitro* measured kinetic parameters and *in silico* measured best distances and frequencies of efficient positions, (see Table 7) the similarity is obvious between increment of distance and decrement of V_{lim} and increment of K_m. There are only two exceptions to this rule. First of them is docking of (S)-warfarin into F114W mutant, where slightly increased distance appears to correlate mainly with decreased V_{lim}, although with both kinetic parameters decreased there is no possible way how it could correlate with both of them. Second one is docking of diclofenac to F114L mutant, where increased distance correlate with increased value of K_m but not with unchanged V_{lim}.

Least accurate comparison of acquired parameter is in case of diclofenac because of very low number of efficient positions from docking (usually around 1 unique position per snapshot) and because for half of mutants only results single activity essay were available (Mosher et al., 2008).

Unfortunately, the frequency and docking energy of catalytically efficient positions between 20 energetically most efficient docking results into each snapshot does not correlate with any kinetic parameters.

Table 7 – Performed mutations and their known kinetic parameters in format V_{lim}/K_m, or activity (in *italics*) where only results of single activity essay are available, compared to wt. Colored according to comparison with best measured distance: green for increased V_{lim} or decreased K_m with decreased distance, red for decreased V_{lim} or increased K_m with decreased distance and gray where only insufficient or highly discutable *in vitro* data are available (Dickmann et al., 2001; Guo et al., 2005; Haining et al., 1996; Haining et al., 1999; Mosher et al., 2008; Tracy et al., 2002).

$\dfrac{V_{lim}}{K_m}$	I359L	F476L	F114L	F114W
(S)-warfarin	lower higher	lower higher	lower higher	lower lower
(R)-warfarin	*lower*		*higher*	
(S)-flurbiprofen	lower higher	lower higher	disputed higher	unchanged unchanged
diclofenac	lower or unchanged higher	*unchanged*	unchanged higher	*higher*

Information about regiospecifity of warfarin hydroxylation cannot be obtained from distances of specific carbon atoms of warfarin enantiomers from heme iron. Ratio of different products of this hydroxylation is surely influenced by different reactivity of each carbon, but there also appears to be strong correlation between ratio of activities towards different products measured *in vitro* and ratio of efficient positions from docking with certain atoms closest to heme iron.

As for hydroxylation of coumarin of (S)-warfarin there is always more positions with closest C-6 than C-8 and more with closest C-7 than C-6 (see Figure 18), though their ratio is significantly smaller than those of *in vitro* activities (compare them with Figure 11).

In hydroxylation of coumarin of (R)-warfarin there was approximately equal number of positions with C-7 and C-6 as closest carbon in wt and F114L mutant, that corresponds well with *in vitro* findings (Haining et al., 1999), while I359L mutants exhibits ratio of C-7 to C-6 positions 14:9, which differs from *in vitro* results, but published amounts of different products of this mutant are too tiny for credible and accurate comparation (Haining et al., 1996).

The ratio of efficient positions with either coumarin or phenyl closer to heme show, that the structures with prevalent hydroxylation on coumarin (wt, I359L and F114W mutants) have (up to almost twice) more efficient positions with coumarin towards the heme. F476L mutant with approximately equal amount of coumarin and phenyl hydroxylated products *in vitro* has also equal amount of positions docked with coumarin or phenyl sides. Finally, F114L is the only mutant with prevalent hydroxylation on phenyl *in vitro* (Mosher et al., 2008; Haining et al., 1999) even though one older study suggest otherwise (Haining et al., 1996). Here, F114L also shows more positions docked with its phenyl than with coumarin ring (see Figure 19).
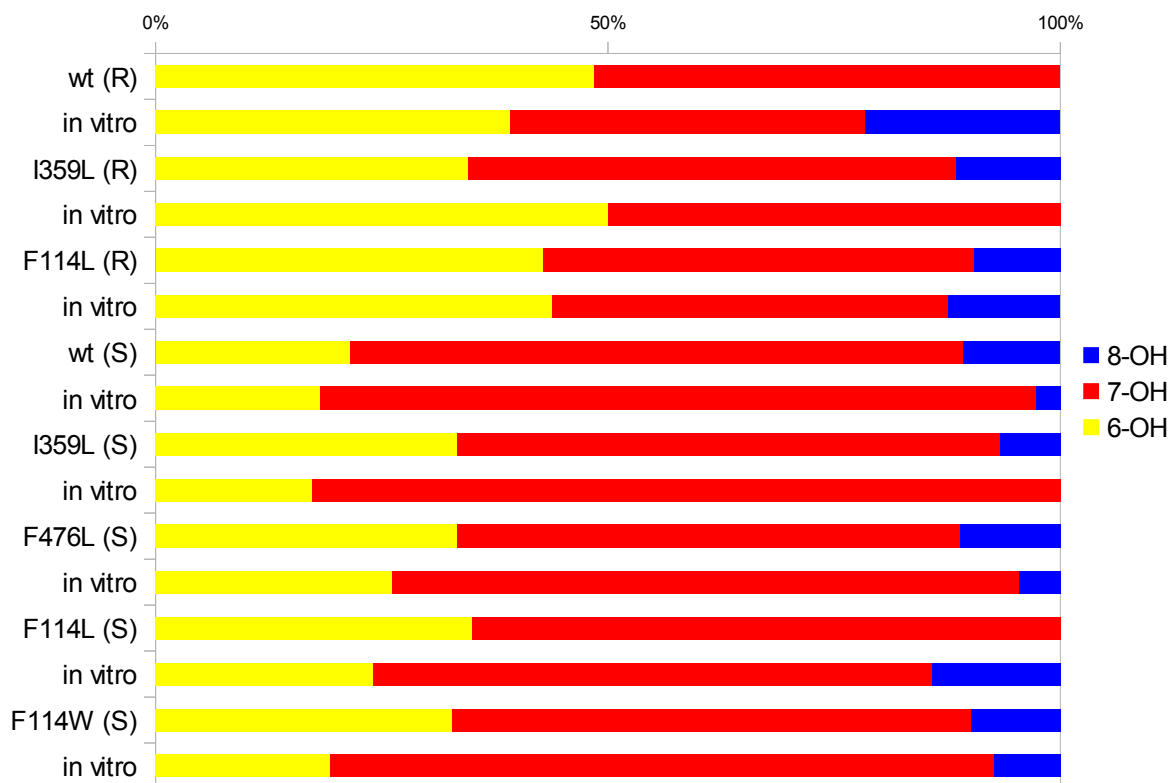
Figure 18 – Ratio of positions of (R)- and (S)-warfarin docking closest with various carbons of coumarin compared to the newest *in vitro* results (Haining et al., 1996; Haining et al., 1999; Mosher et al., 2008).
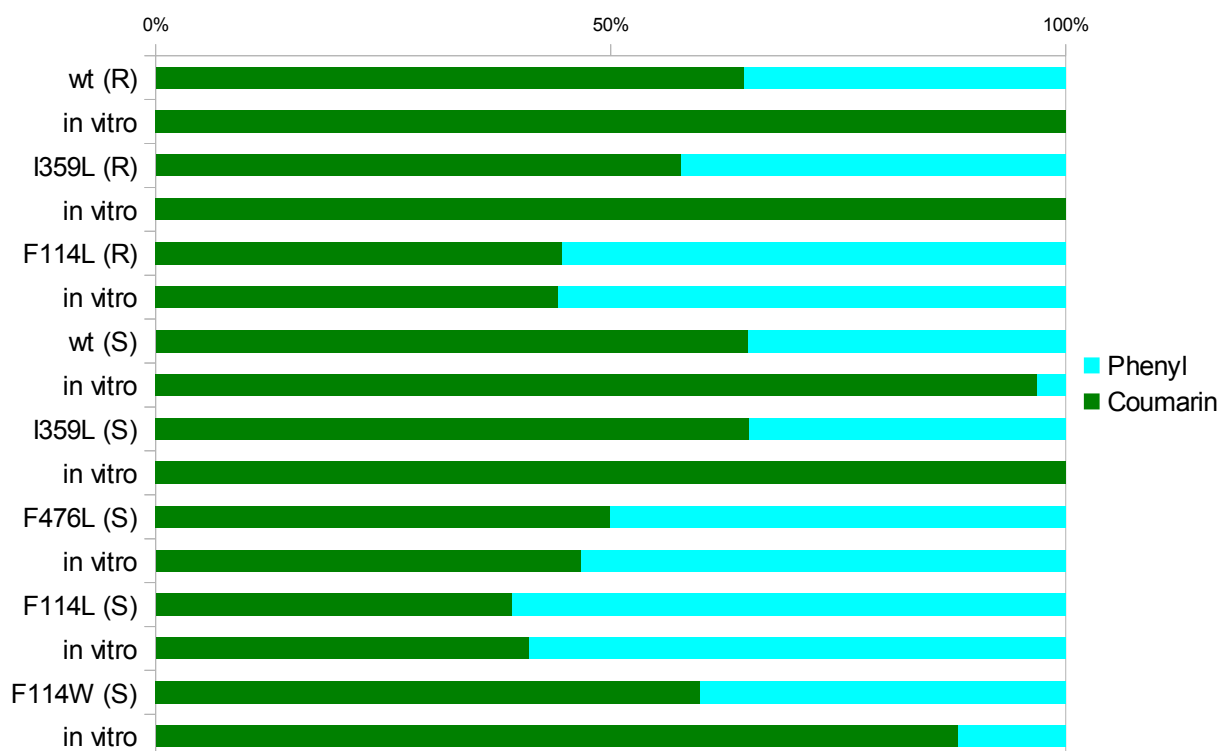

Figure 19 – Ratio of positions of (R)- and (S)-warfarin docking closest with either coumarin or phenyl ring compared to the newest *in vitro* results (Haining et al., 1996; Haining et al., 1999; Mosher et al., 2008).

6 Conclusions

Structures of wild type CYP 2C9 and its five mutants I359L, F476L, F114L, F114W and R97F were prepared from crystal structure of construct 1OG2 (Williams et al., 2003). 100 ns long MD simulations were performed to probe mutants' stability and flexibility. Four drugs were chosen for docking study: NSAIDs (S)-flurbiprofen and diclofenac, anticoagulant (S)-warfarin and its enantiomer (R)-warfarin. These four ligands were docked into rigid snapshots acquired from trajectories.

All studied structures were stable with the anticipated exception of R97F mutant, where heme started to slide away from cavity and outside the enzyme proving earlier suggested (Dickmann et al., 2004) the key role of Arg97 in hydrogen bonding of heme propionates.

Most important and strongly prevalent type of interaction between ligand and CYP 2C9 active site seems to be hydrophobic interaction with residues Leu362, Leu366, Val113 and Ala297 near the heme and with mostly Leu208, Phe114 and Phe476 farther from it. Best distances in which have all ligands docked into wt were from 2.9 Å to 3.6 Å, while best distances of docking into mutants were usually longer up to 6.1 Å.

Significant and clinically important drop of activity of I359L mutant (know as 3* allele) is caused only by transition of Leu361 and Leu362 about 2 Å into cavity reducing volume of its lower part, that leads to increased distances in which ligands bind to heme iron by about 1.3 Å.

Although earlier *in vitro* studies tried to prove importance of π-stacking between aromatic rings of ligands and Phe114 and Phe476 (Mosher et al., 2008; Haining et al., 1999), results of this study suggest that π-stacking is only rarely present and that observed changes in activity of these mutants are caused by redesign of active site cavity architecture, mostly by increased overlap of heme by I-helix and by various changes of shape of loop after K-helix, while mutated residues retains the position, orientation and function of original residues. While these changes do not significantly alter interacting residues in both Phe to Leu mutants, they result in reduction of volume of lower part of cavity and also in prolongations of distances of all ligands from heme iron. In F114W on the other hand is cavity volume not so significantly reduced, but great change in shape of loop after K-helix pushes Leu362 away from cavity and its function is undertaken by Pro363. This results in the shortest measured distances from heme within studied mutants.

Results of this study appears to be in great accordance with previous *in vitro* results. Strong correlation between distance from iron to hydroxylated carbon and both main kinetic parameters V_{lim} and K_m was observed for all studied ligands. On the other hand, the number of efficient positions is dependent also on other factors like size of the cavity and therefore cannot be used for compare of individual structures, but it still provides relatively good agreement with regiospecificity in CYP 2C9 mutant structures.

References

Anzenbacher P., Anzenbacherová E. (2001) Cytochromes P450 and metabolism of xenobiotics. *Cell. Mol. Life Sci.* **58**, 737-47.

Berendsen H. J. C., Grigera J. R., Straatsma T. P. (1987) The missing term in effective pair potentials. *J. Phys. Chem.* **91**, 6269-6271.

Bernstein F. C., Koetzle T. F., Williams G. J., Meyer Jr. E. E., Brice M. D., Rodgers J. R., Kennard O., Shimanouchi T., Tasumi M. (1977) The Protein Data Bank: A computer-based archival file for macromolecular structures *J. Mol. Biol.*, **112**: 535.

Blaisdell J., Jorge-nebert L. F., Coulter S., Ferguson S. S., Lee S.-jun, Chanas B., Xi T., Mohrenweiser H., Ghanayem B., Goldstein J. A. (2004) Discovery of new potentially defective alleles of human CYP2C9. *Pharmacogenetics* **14**, 527-537.

Coutsias E. A., Chaok S., Dill K. A. (2004) Using quaternions to calculate RMSD. *J. Comput. Chem.* **25**, 1849-1857.

Danielson P. B. (2002) The Cytochrome P450 Superfamily: Biochemistry, evolution and drug metabolism in humans. *Curr. Drug Metab.* **3**, 561-97.

Dastidar S. G., Ganguly K., Chaudhuri K., Chakrabarty A. N. (2000) The anti-bacterial action of diclofenac shown by inhibition of DNA synthesis. *Int. J. Antimicrob. Agents* 14, 249-51.

Denisov I. G., Makris T. M., Sligar S. G., Schlichting I. (2005) Structure and chemistry of cytochrome P450. *Chem. Rev.* **105**, 2253-77.

Dickmann L. J., Locuson C. W., Jones J. P., Rettie A. E. (2004) Differential roles of Arg97, Asp293, and Arg108 in enzyme stability and substrate specificity of CYP2C9. *Mol. Pharmacol.* **65**, 842-50.

Dickmann L. J., Rettie a E., Kneller M. B., Kim R. B., Wood A. J. J., Stein C. M., Wilkinson G. R., Schwarz U. I. (2001) Identification and functional characterization of a new CYP2C9 variant (CYP2C9*5) expressed among African Americans. *Mol. Pharmacol.* **60**, 382-7.

Ditzler M., Otyepka M., Šponer J., Walter N. (2010) Molecular Dynamics and Quantum Mechanics of RNA: Conformational and Chemical Change We Can Believe In. *Acc. Chem. Res.*, **43**, 40-47.

Dundas J., Ouyang Z., Tseng J., Binkowski A., Turpaz Y., Liang J. (2006) CASTp: computed atlas of surface topography of proteins with structural and topographical mapping of functionally annotated resiudes. *Nucleic Acid Research* **34**, 116-118.

Geer L. Y., Marchler-Bauer A., Geer R. C., Han L., He J., He S., Liu C., Shi W., Bryant S. H. (2010) The NCBI BioSystems database. *Nucleic Acids Res.* **38**, D492-6.

Goldstein J. A. (2001) Clinical relevance of genetic polymorphisms in the human CYP2C subfamily. *Br. J. Clin. Pharmacol.* **52**, 349-55.

Guo Y., Wang Y., Si D., Fawcett P. J., Zhong D., Zhou H. (2005) Catalytic activities of human cytochrome P450 2C9*1, 2C9*3 and 2C9*13. *Xenobiotica* **35**, 853-861.

Haining R. L., Hunter a P., Veronese M. E., Trager W. F., Rettie A. E. (1996) Allelic variants of human

cytochrome P450 2C9: baculovirus-mediated expression, purification, structural characterization, substrate stereoselectivity, and prochiral selectivity of the wild-type and I359L mutant forms. *Arch. Biochem. Biophys.* **333**, 447-58.

Haining R. L., Jones J. P., Henne K. R., Fisher M. B., Koop D. R., Trager W. F., Rettie A. E. (1999) Enzymatic determinants of the substrate specificity of CYP2C9: role of B'-C loop residues in providing the pi-stacking anchor site for warfarin binding. *Biochemistry* **38**, 3285-92.

Hess B., van der Spoel D., Lindahl E., Apol E., Apostolov R., Berendsen H. J. C., van Buuren A., Bjelmark P., van Drunen R., Feenstra A., Groenhof G., Kasson P., Larsson P., Meulenhoff P., Murtola T., Páll S., Pronk S., Schulz R., Shirts M., Sijbers A., Tieleman P. (downloaded 2/6/2012 from http://www.gromacs.org), pp. 1-5.

Hess B., van der Spoel D., Lindahl E., Apol E., Apostolov R., Berendsen H. J. C., van Buuren A., Bjelmark P., van Drunen R., Feenstra A., Groenhof G., Kasson P., Larsson P., Meulenhoff P., Murtola T., Páll S., Pronk S., Schulz R., Shirts M., Sijbers A., Tieleman P. (downloaded 2/6/2012 from http://www.gromacs.org), pp. 5-6.

Hess B., van der Spoel D., Lindahl E., Apol E., Apostolov R., Berendsen H. J. C., van Buuren A., Bjelmark P., van Drunen R., Feenstra A., Groenhof G., Kasson P., Larsson P., Meulenhoff P., Murtola T., Páll S., Pronk S., Schulz R., Shirts M., Sijbers A., Tieleman P. (downloaded 2/6/2012 from http://www.gromacs.org), pp. 210-211.

Hummel M. A., Gannett P. M., Aguilar J. S., Tracy T. S. (2004) Effector-Mediated Alteration of Substrate Orientation in Cytochrome P450 2C9. *Biochemistry* **43**, 7207-7214.

Humphrey W., Dalke A., Schulten K. (1996) VMD: Visual Molecular Dynamics. *J. Mol. Graph.* **14**, 33-38.

Kirchheiner J., Brockmöller J. (2005) Clinical consequences of cytochrome P450 2C9 polymorphism. *Clin. Pharmacol. Ther.* **77**, 1-16.

Miners J. O., Birkett D. J. (1998) Cytochrome P4502C9: an enzyme of major importance in human drug metabolism. *Br. J. Clin. Pharmacol.* **45**, 525-538.

Morris G. M., Goodsell D. S., Halliday R. S., Huey R., Hart W. E., Belew R. K., Olson A. J. (1998) Automated docking using a lamarckian genetic algorithm and empirical binding free energy function. J. Comput. Chem. 19, 1639-1662.

Mosher C. M., Hummel M. A., Tracy T. S., Rettie A. E. (2008) Functional analysis of phenylalanine residues in the active site of cytochrome P450 2C9. *Biochemistry* **47**, 11725-34.

Nezbeda I., Kolafa J. and Kotrla M. (2002) Úvod do počítacových simulací – Metody Monte Carlo a molekulární dynamiky, pp. 205, Karolinum, Praha.

Oostenbrink C., Villa A., Mark A. E., van Gunsteren W. F. (2004) A biomolecular force field based on the free enthalpy of hydration and solvation: The GROMOS force-field parameter sets 53A5 and 53A6. *J. Comput. Chem.* **25**, 1656-76.

Otyepka M., Berka K., Anzenbacher P. (2012) Is there a relationship between the substrate preferences and structural flexibility of cytochromes P450? *Curr. Drug Metab.* **13**, 130-142.

Preissner S., Kroll K., Dunkel M., Goldsobel G., Kuzmann D., Senger S., Günther S., Winnenburg R.,

Schroeder M., Preissner R. (2010) SuperCYP: a comprehensive database on Cytochrome P450 enzymes including a tool for analysis of CYP-drug interactions. *Nucleic Acids Res.* **38**, D237-43.

Ridderström M., Masimirembwa C., Trump-Kallmeyer S., Ahlefelt M., Otter C., Andersson T. B. (2000) Arginines 97 and 108 in CYP2C9 are important determinants of the catalytic function. *Biochem. Biophys. Res. Commun.* **270**, 983-7.

Rydberg P., Gloriam D. E., Olsen L. (2010) The SMARTCyp cytochrome P450 metabolism prediction server. *Bioinformatics* **26**, 2988-2989.

Rydberg P., Gloriam D. E., Zaretzki J., Breneman C., Olsen L. (2010) SMARTCyp: A 2D Method for Prediction of Cytochrome P450-Mediated Drug Metabolism. *ACS Med. Chem. Lett.* **1**, 96-100.

Rydberg P., Jørgensen M. S., Jacobsen T. A., Jacobsen A.-M., Madsen K. G., Olsen L. (2013) Nitrogen Inversion Barriers Affect the N-Oxidation of Tertiary Alkylamines by Cytochromes P450. *Angewandte Chemie International Edition* **52**, 993-997.

Rydberg P., Olsen L. (2012) Ligand-Based Site of Metabolism Prediction for Cytochrome P450 2D6. *ACS Med. Chem. Lett.* **3**, 69-73.

Rydberg P., Olsen L. (2012) Predicting Drug Metabolism by Cytochrome P450 2C9: Comparison with the 2D6 and 3A4 Isoforms. *ChemMedChem* **7**, 1202-1209.

Rydberg P., Rostkowski M., Gloriam D. E., Olsen L. (2013) The Contribution of Atom Accessibility to Site of Metabolism Models for Cytochromes P450. *Mol. Pharm.* **10**, 1216-1223.

Sanner M. (1999) Python: A programming language for software integration and development. *J. Mol. Graph. Model.* **17**, 57-61.

Schrödinger (2011) The PyMOL Molecular Graphics System, Version 1.4rc, LLC.

Sim S. C., Ingelman-Sundberg M. (2010) The Human Cytochrome P450 (CYP) Allele Nomenclature website: a peer-reviewed database of CYP variants and their associated effects *Hum. Genomics.* **4**, 278-81.

Sullivan T. H., Ghanayem B. I., Bell D. A., Zhang Z., Kaminsky L. S., Shenfield G. M., Miners J. O., Birkett D. J., Goldstein J. A. (1996) The role of the CYP2C9-Ile[359] allelic variant in the tolbutamide polymorphism. *Pharmacogenetics* **6**, 341-349.

Tracy T. S., Hutzler J. M., Haining R. L., Rettie A. E., Hummel M. A., Dickmann L. J. (2002) Polymorphic variants (CYP2C9*3 and CYP2C9*5) and the F114L active site mutation of CYP2C9: effect on atypical kinetic metabolism profiles. *Drug Metab. Dispos.* **30**, 385-390.

Trott O., Olson A. J. (2010) AutoDock Vina: improving the speed and accuracy of docking with a new scoring function, efficient optimization and multithreading. *J. Comput. Chem.* **31**, 455-461.

van Gunsteren W.F., Mark A.E. (1998) Validation of molecular dynamics simulation. *J. Chem. Phys.* **108**, 6109-6116.

Voet D., Voetová J. G. (1995) Biochemie, pp. 156-158, Victoria Publishing, Praha, Czech Republic.

Wardrop D., Keeling D. (2008) The story of the discovery of heparin and warfarin. *Br. J. Haematol.* **141**, 757-63.

Wester M. R., Yano J. K., Schoch G. A., Yang C., Griffin K. J., Stout C. D., Johnson E. F. (2004) The structure of human cytochrome P450 2C9 complexed with flurbiprofen at 2.0-Å resolution. *J. Biol. Chem.* **279**, 35630-35637.

Williams P. A., Cosme J., Ward A., Angove H. C., Jhoti H. (2003) Crystal structure of human cytochrome P450 2C9 with bound warfarin. *Nature* **424**, 464-468.

List of Figures

Abbreviations

CYP	cytochrome P450
CYP2C9	cytochrome P450 2C9
wt	wild-type
X83Y	point mutation of amino acid X for aminoacid Y at position 83
NSAID	nonsteroidal anti-inflamatory drug

Color Chart

Carbon	
highlighted	
Chlorine	
Fluorine	
Hydrogen	
Iron	
Nitrogen	
Oxygen	
Sulphur	

7 Appendices

Appendix A
Table A1 – Mutations and their effect on substrate specifity of cytochrome P450 2C9 from literature. *Higher* stands for either activity or V(lim) more than 110% of wt, *Identical* for 90 to 110%, *Lower* for 50 to 90%, *Poor* for 20 to 50%, *Very low* for 4 to 20%, *Zero* for lower than 4% and *Other* for another important kind of information in reference. Essays are annotated as *sil* (*in silico*), *vit* (*in vitro*) and *viv* (*in vivo*).

Mutant			
Activity (V$_{lim}$)	**Assay**	**Drug**	**Reference**
A477T			
Poor	vit	diclofenac	Maekawa et al., 2006
D293N			
Very low	vit	diclofenac	Dickmann et al., 2004
Very low	vit	pyrene	Dickmann et al., 2004
Very low	vit	warfarin (S)	Dickmann et al., 2004
D293V			
Zero	vit	diclofenac	Dickmann et al., 2004
Very low	vit	pyrene	Dickmann et al., 2004
Zero	vit	warfarin (S)	Dickmann et al., 2004
D360E			
Lower	vit	diclofenac	Dickmann et al., 2001
Very low	vit	flurbiprofen (S)	Tracy et al., 2002
Poor	vit	lauric acid	Dickmann et al., 2001
Poor	vit	naproxen (S)	Tracy et al., 2002
Poor	vit	piroxicam	Tracy et al., 2002
Lower	vit	warfarin ((S)-7-OH)	Dickmann et al., 2001
E104A			
Lower	vit	diclofenac	Ridderström et al., 2000
E272G			
Lower	vit	tolbutamide	Blaisdell et al., 2004
F100A			
Higher	vit	diclofenac	Ridderström et al., 2000
F100L			
Higher	vit	diclofenac	Mosher et al., 2008
Higher	vit	flurbiprofen (S)	Mosher et al., 2008
Higher	vit	warfarin ((S)-4'-OH)	Mosher et al., 2008

Higher	vit	warfarin (S)	Mosher et al., 2008
Higher	vit	warfarin ((S)-6-OH)	Mosher et al., 2008
Higher	vit	warfarin ((S)-7-OH)	Mosher et al., 2008
Higher	vit	warfarin ((S)-8-OH)	Mosher et al., 2008
F110L			
other	vit	arachidonic acid	Haining et al., 1999
Lower	vit	diclofenac	Haining et al., 1999
Identical	vit	lauric acid	Haining et al., 1999
Higher	vit	warfarin (R)	Haining et al., 1999
Higher	vit	warfarin (S)	Haining et al., 1999
F110Y			
Poor	vit	lauric acid	Haining et al., 1999
Poor	vit	warfarin (S)	Haining et al., 1999
F114L			
other	vit	arachidonic acid	Haining et al., 1999
Identical	vit	diclofenac	Haining et al., 1999
Identical	vit	diclofenac	Mosher et al., 2008
Lower	vit	flurbiprofen (S)	Mosher et al., 2008
Higher	vit	flurbiprofen (S)	Tracy et al., 2002
Lower	vit	lauric acid	Haining et al., 1999
Identical	vit	naproxen (S)	Tracy et al., 2002
Lower	vit	piroxicam	Tracy et al., 2002
Higher	vit	warfarin ((S)-4'-OH)	Mosher et al., 2008
Very low	vit	warfarin (S)	Mosher et al., 2008
Zero	vit	warfarin ((S)-6-OH)	Mosher et al., 2008
Zero	vit	warfarin ((S)-7-OH)	Mosher et al., 2008
Lower	vit	warfarin ((S)-8-OH)	Mosher et al., 2008
Higher	vit	warfarin (R)	Haining et al., 1999
Very low	vit	warfarin (S)	Haining et al., 1999
F114L/F476L			
Lower	vit	diclofenac	Mosher et al., 2008
Poor	vit	flurbiprofen (S)	Mosher et al., 2008
Higher	vit	warfarin ((S)-4'-OH)	Mosher et al., 2008
Very low	vit	warfarin (S)	Mosher et al., 2008
Zero	vit	warfarin ((S)-6-OH)	Mosher et al., 2008

Zero	vit	warfarin ((S)-7-OH)	Mosher et al., 2008
Poor	vit	warfarin ((S)-8-OH)	Mosher et al., 2008

F114W

Higher	vit	diclofenac	Mosher et al., 2008
Identical	vit	flurbiprofen (S)	Mosher et al., 2008
Higher	vit	warfarin ((S)-4'-OH)	Mosher et al., 2008
Poor	vit	warfarin (S)	Mosher et al., 2008
Poor	vit	warfarin ((S)-6-OH)	Mosher et al., 2008
Poor	vit	warfarin ((S)-7-OH)	Mosher et al., 2008
Identical	vit	warfarin ((S)-8-OH)	Mosher et al., 2008

F114W/F476W

Identical	vit	diclofenac	Mosher et al., 2008
Poor	vit	flurbiprofen (S)	Mosher et al., 2008
Higher	vit	warfarin ((S)-4'-OH)	Mosher et al., 2008
Identical	vit	warfarin (S)	Mosher et al., 2008
Lower	vit	warfarin ((S)-6-OH)	Mosher et al., 2008
Identical	vit	warfarin ((S)-7-OH)	Mosher et al., 2008
Identical	vit	warfarin ((S)-8-OH)	Mosher et al., 2008

F476L

Identical	vit	diclofenac	Mosher et al., 2008
Lower	vit	flurbiprofen (S)	Mosher et al., 2008
Higher	vit	warfarin ((S)-4'-OH)	Mosher et al., 2008
Poor	vit	warfarin (S)	Mosher et al., 2008
Zero	vit	warfarin ((S)-6-OH)	Mosher et al., 2008
Very low	vit	warfarin ((S)-7-OH)	Mosher et al., 2008
Poor	vit	warfarin ((S)-8-OH)	Mosher et al., 2008

F476W

Lower	vit	diclofenac	Mosher et al., 2008
Poor	vit	flurbiprofen (S)	Mosher et al., 2008
Higher	vit	warfarin ((S)-4'-OH)	Mosher et al., 2008
Higher	vit	warfarin (S)	Mosher et al., 2008
Higher	vit	warfarin ((S)-6-OH)	Mosher et al., 2008
Higher	vit	warfarin ((S)-7-OH)	Mosher et al., 2008
Higher	vit	warfarin ((S)-8-OH)	Mosher et al., 2008

H251R

Lower	vit	tolbutamide	Blaisdell et al., 2004

I359L

Very low	vit	2-naphtyl methyl sulfide	Haining et al., 1996
Very low	vit	celecoxib	Tang et al., 2001
Poor	viv	celecoxib	Kirchheiner et al., 2003b
Poor	vit	cyclophosphamide	Griskevicius et al., 2003
Lower	viv	cyclophosphamide	Griskevicius et al., 2003
Poor	vit	diclofenac	Dickmann et al., 2001
Identical	vit	diclofenac	Guo et al., 2005b
Higher	viv	diclofenac	Kirchheiner et al., 2003a
Very low	vit	flurbiprofen (S)	Tracy et al., 2002
Poor	viv	fluvastatin ((-)-3S,5R)	Kirchheiner et al., 2003c
Lower	viv	fluvastatin ((+)-3R,5S)	Kirchheiner et al., 2003c
Poor	viv	glyburide	Kirchheiner et al., 2002b
Very low	vit	ketobemidone	Yasar et al., 2005
Poor	viv	ketobemidone	Yasar et al., 2005
Very low	vit	lauric acid	Dickmann et al., 2001
Poor	vit	lornoxicam	Guo et al., 2005a
Poor	vit	lornoxicam	Iida et al., 2004
Very low	viv	lornoxicam	Iida et al., 2004
Poor	viv	losartan	Yasar et al., 2002
Very low	vit	luciferin H	Guo et al., 2005b
Very low	vit	naproxen (S)	Tracy et al., 2002
Very low	vit	p-tolyl methyl sulfide	Haining et al., 1996
Very low	vit	perazine	Störmer et al., 2000
Poor	viv	phenytoin	Rosemary et al., 2006
Very low	vit	piroxicam	Tracy et al., 2002
Identical	vit	tolbutamide	Guo et al., 2005b
Very low	viv	tolbutamide	Kirchheiner et al., 2002a
Poor	viv	torsemide	Vormfelde et al., 2004
Very low	vit	warfarin ((S)-6-OH)	Haining et al., 1996
Very low	vit	warfarin ((S)-7-OH)	Dickmann et al., 2001
Very low	vit	warfarin ((S)-7-OH)	Haining et al., 1996

I99H

Higher	vit	diclofenac	Ridderström et al., 2000

I99H/S220P/P221T/S286N/N289I/V292A/F295L			
other	vit	mephenytoin (S)	Tsao et al., 2001
I99H/S220P/P221T/S286N/V292A/F295L			
other	vit	mephenytoin (S)	Tsao et al., 2001
I99H/V292A/F295L/I331V			
Lower	vit	diclofenac	Niwa et al., 2002
Lower	vit	tolbutamide	Niwa et al., 2002
K72E			
other	vit	diclofenac	Davies et al., 2004
other	vit	ibuprofen	Davies et al., 2004
K72L			
other	vit	diclofenac	Davies et al., 2004
other	vit	ibuprofen	Davies et al., 2004
K72Q			
other	vit	diclofenac	Davies et al., 2004
other	vit	ibuprofen	Davies et al., 2004
K72V			
other	vit	diclofenac	Davies et al., 2004
other	vit	ibuprofen	Davies et al., 2004
L102A			
Higher	vit	diclofenac	Ridderström et al., 2000
L17I			
Lower	vit	diclofenac	Maekawa et al., 2006
L19I			
Identical	vit	tolbutamide	Blaisdell et al., 2004
L208V			
Lower	viv	warfarin	Leung et al., 2001
L90P			
other	sil	diclofenac	Zhou et al., 2006
Very low	vit	diclofenac	Guo et al., 2005b
other	sil	lornoxicam	Zhou et al., 2006
Very low	vit	lornoxicam	Guo et al., 2005a
Zero	vit	luciferin H	Guo et al., 2005b
Identical	vit	tolbutamide	Guo et al., 2005b
N107A			

Lower	vit	diclofenac	Ridderström et al., 2000

P279T

Lower	vit	diclofenac	Maekawa et al., 2006

P382S

Lower	vit	tolbutamide	DeLozier et al., 2005

P489S

Lower	vit	tolbutamide	Blaisdell et al., 2004

Q214L

Poor	vit	diclofenac	Maekawa et al., 2006

Q454H

Lower	vit	tolbutamide	DeLozier et al., 2005

R105A

Poor	vit	diclofenac	Ridderström et al., 2000

R105F

Poor	vit	diclofenac	Dickmann et al., 2004
Very low	vit	pyrene	Dickmann et al., 2004
Very low	vit	warfarin (S)	Dickmann et al., 2004

R105H

Lower	vit	diclofenac	Dickmann et al., 2004
Poor	vit	pyrene	Dickmann et al., 2004
Poor	vit	warfarin (S)	Dickmann et al., 2004

R108A

Zero	vit	diclofenac	Ridderström et al., 2000

R108E

Zero	vit	diclofenac 4'-OH	Tai et al., 2008
other	vit	ibuprofen amine	Tai et al., 2008
other	vit	propanolol	Tai et al., 2008
Identical	vit	pyrene 1-OH	Tai et al., 2008
Very low	vit	warfarin ((R)-7-OH)	Tai et al., 2008

R108E/D293N

Very low	vit	diclofenac 4'-OH	Tai et al., 2008
other	vit	ibuprofen amine	Tai et al., 2008
other	vit	propanolol	Tai et al., 2008
Poor	vit	pyrene 1-OH	Tai et al., 2008
Very low	vit	warfarin ((S)-7-OH)	Tai et al., 2008

R108F			
Zero	vit	diclofenac	Dickmann et al., 2004
Lower	vit	pyrene	Dickmann et al., 2004
Zero	vit	warfarin (S)	Dickmann et al., 2004
R108H			
Zero	vit	diclofenac	Dickmann et al., 2004
Very low	vit	pyrene	Dickmann et al., 2004
Zero	vit	warfarin (S)	Dickmann et al., 2004
R125H			
Poor	vit	tolbutamide	DeLozier et al., 2005
R132Q			
Very low	vit	diclofenac	Yin et al., 2008
R144C			
Lower	viv	acenocoumarol	Visser et al., 2004
Poor	vit	celecoxib	Tang et al., 2001
Higher	viv	celecoxib	Kirchheiner et al., 2003b
Lower	vit	cyclophosphamide	Griskevicius et al., 2003
Higher	viv	cyclophosphamide	Griskevicius et al., 2003
Higher	viv	diclofenac	Kirchheiner et al., 2003c
Lower	viv	fluvastatin ((-)-3S,5R)	Kirchheiner et al., 2003c
Lower	viv	fluvastatin ((+)-3R,5S)	Kirchheiner et al., 2003c
Lower	viv	glyburide	Kirchheiner et al., 2002b
Poor	vit	ketobemidone	Yasar et al., 2005
Higher	vit	lornoxicam	Iida et al., 2004
Identical	viv	losartan	Yasar et al., 2002
Lower	vit	perazine	Störmer et al., 2000
Lower	viv	phenprocoumon	Visser et al., 2004
Lower	vit	tolbutamide	Yamazaki et al., 1998
Lower	viv	tolbutamide	Kirchheiner et al., 2002a
Lower	viv	tolbutamide	Rettie et al., 1994
Lower	viv	torsemide	Vormfelde et al., 2004
Poor	vit	warfarin ((R)-7-OH)	Yamazaki et al., 1998
Very low	vit	warfarin ((S)-6-OH)	Yamazaki et al., 1998
Zero	viv	warfarin ((S)-6-OH)	Rettie et al., 1994
Very low	vit	warfarin ((S)-7-OH)	Yamazaki et al., 1998

Very low	viv	warfarin ((S)-7-OH)	Rettie et al., 1994
R150H			
Higher	vit	tolbutamide	Blaisdell et al., 2004
R150L			
Identical	vit	diclofenac	Maekawa et al., 2006
R335Q			
Lower	vit	diclofenac	Yin et al., 2008
R335W			
Poor	vit	tolbutamide	Blaisdell et al., 2004
R97A			
Higher	vit	diclofenac	Ridderström et al., 2000
other	vit, sil	other	Davies et al., 2004
R97F			
other	vit, sil	other	Davies et al., 2004
Zero	vit	diclofenac	Dickmann et al., 2004
Zero	vit	pyrene	Dickmann et al., 2004
Zero	vit	warfarin (S)	Dickmann et al., 2004
R97H			
Very low	vit	diclofenac	Dickmann et al., 2004
Zero	vit	pyrene	Dickmann et al., 2004
Zero	vit	warfarin (S)	Dickmann et al., 2004
R97I			
other	vit, sil	other	Davies et al., 2004
R97K			
other	vit, sil	other	Davies et al., 2004
R97L			
other	vit, sil	other	Davies et al., 2004
R97P			
other	vit, sil	other	Davies et al., 2004
R97Q			
other	vit, sil	other	Davies et al., 2004
R97T			
other	vit, sil	other	Davies et al., 2004
R97V			
other	vit, sil	other	Davies et al., 2004

S95A			
Lower	vit	diclofenac	Ridderström et al., 2000
T130R			
Very low	vit	diclofenac	Maekawa et al., 2006
T299A			
Poor	vit	tolbutamide	DeLozier et al., 2005
V113L			
Lower	vit	lauric acid	Haining et al., 1999
Zero	vit	warfarin (S)	Haining et al., 1999

Table References

Blaisdell J., Jorge-nebert L. F., Coulter S., Ferguson S. S., Lee S.-jun, Chanas B., Xi T., Mohrenweiser H., Ghanayem B., Goldstein J. A. (2004) Discovery of new potentially defective alleles of human CYP2C9. *Pharmacogenetics* **14**, 527-537.

Davies C., Witham K., Scott J. R., Pearson A., DeVoss J. J., Graham S. E., Gillam E. M. J. (2004) Assessment of arginine 97 and lysine 72 as determinants of substrate specificity in cytochrome P450 2C9 (CYP2C9). *Drug Metab. Dispos.* **32**, 431-6.

Delozier T. C., Lee S.-chin, Coulter S. J., Goh B. C., Goldstein J. A. (2005) Functional characterization of novel allelic variants of CYP2C9 recently discovered in Southeast Asians. *Environ. Health* **315**, 1085-1090.

Dickmann L. J., Rettie a E., Kneller M. B., Kim R. B., Wood A. J. J., Stein C. M., Wilkinson G. R., Schwarz U. I. (2001) Identification and functional characterization of a new CYP2C9 variant (CYP2C9*5) expressed among African Americans. *Mol. Pharmacol.* **60**, 382-7.

Dickmann L. J., Locuson C. W., Jones J. P., Rettie A. E. (2004) Differential roles of Arg97, Asp293, and Arg108 in enzyme stability and substrate specificity of CYP2C9. *Mol. Pharmacol.* **65**, 842-50.

Griskevicius L., Yasar U., Sandberg M., Hidestrand M., Eliasson E., Tybring G., Hassan M., Dahl M.-L. (2003) Bioactivation of cyclophosphamide: the role of polymorphic CYP2C enzymes. *Eur. J. Clin. Pharmacol.* **59**, 103-9.

Guo Y., Zhang Y., Wang Y., Chen X., Si D., Zhong D., Fawcett J. P., Zhou H. (2005) Role of CYP2C9 and its variants (CYP2C9*3 and CYP2C9*13) in the metabolism of lornoxicam in humans. *Drug Metab. Dispos.* **33**, 749-753.

Guo Y., Wang Y., Si D., Fawcett P. J., Zhong D., Zhou H. (2005) Catalytic activities of human cytochrome P450 2C9*1, 2C9*3 and 2C9*13. *Xenobiotica* **35**, 853-861.

Haining R. L., Hunter a P., Veronese M. E., Trager W. F., Rettie A. E. (1996) Allelic variants of human cytochrome P450 2C9: baculovirus-mediated expression, purification, structural characterization, substrate stereoselectivity, and prochiral selectivity of the wild-type and I359L mutant forms. *Arch. Biochem. Biophys.* **333**, 447-58.

Haining R. L., Jones J. P., Henne K. R., Fisher M. B., Koop D. R., Trager W. F., Rettie A. E. (1999) Enzymatic determinants of the substrate specificity of CYP2C9: role of B'-C loop residues in providing the pi-stacking anchor site for warfarin binding. *Biochemistry* **38**, 3285-92.

Iida I., Miyata A., Arai M., Hirota M., Akimoto M., Higuchi S., Kobayashi K., Chiba K. (2004) Catalytic roles of CYP2C9 and its variants (CYP2C9*2 and CYP2C9*3) in lornoxicam 5'-hydroxylation. *Drug Metab. Dispos.* **32**, 7-9.

Kirchheiner J., Bauer S., Meineke I., Rohde W., Prang V., Meisel C., Roots I., Brockmöller J. (2002) Impact of CYP2C9 and CYP2C19 polymorphisms on tolbutamide kinetics and the insulin and glucose response in healthy volunteers. *Pharmacogenetics* **12**, 101-109.

Kirchheiner J., Brockmöller J., Meineke I., Bauer S., Rohde W., Meisel C., Roots I. (2002) Impact of CYP2C9 amino acid polymorphisms on glyburide kinetics and on the insulin and glucose response in healthy volunteers. *Clin. Pharmacol. Ther.* **71**, 286-96.

Kirchheiner J., Kudlicz D., Meisel C., Bauer S., Meineke I., Roots I., Brockmöller J. (2003) Influence of CYP2C9 polymorphisms on the pharmacokinetics and cholesterol-lowering activity of (-)-3S,5R-fluvastatin and (+)-3R,5S-fluvastatin in healthy volunteers. *Clin. Pharmacol. Ther.* **74**, 186-94.

Kirchheiner J., Meineke I., Steinbach N., Meisel C., Roots I., Brockmöller J. (2003) Pharmacokinetics of diclofenac and inhibition of cyclooxygenases 1 and 2: no relationship to the CYP2C9 genetic polymorphism in humans. *Br. J. Clin. Pharmacol.* **55**, 51-61.

Kirchheiner J., Störmer E., Meisel C., Steinbach N., Roots I., Brockmöller J. (2003) Influence of CYP2C9 genetic polymorphisms on pharmacokinetics of celecoxib and its metabolites. *Pharmacogenetics* **144**, 473-480.

Leung A. Y. H., Chow H. C. H., Kwong Y. L., Lie A. K. W., Fung A. T. K., Chow W. H., Yip A. S. B., Liang R. (2001) Genetic polymorphism in exon 4 of cytochrome P450 CYP2C9 may be associated with warfarin sensitivity in Chinese patients. *Blood* **98**, 2584-2587.

Maekawa K., Fukushima-Uesaka H., Tohkin M., Hasegawa R., Kajio H., Kuzuya N., Yasuda K., Kawamoto M., Kamatani N., Suzuki K., Yanagawa T., Yoshiro S., Sawada J.-i. (2006) Four novel defective alleles and comprehensive haplotype analysis of CYP2C9 in Japanese. *Pharmacogenet. Genomics* **16**, 497-514.

Mosher C. M., Hummel M. A., Tracy T. S., Rettie A. E. (2008) Functional analysis of phenylalanine residues in the active site of cytochrome P450 2C9. *Biochemistry* **47**, 11725-34.

Niwa T., Kageyama A., Kishimoto K., Yabusaki Y., Ishibashi F., Katagiri M. (2002) Amino acid residues affecting the activities of human cytochrome P450 2C9 and 2C19. *Drug Metab. Dispos.* **30**, 931-936.

Rettie A.E., Wienkers L. C., Gonzalez F. J., Trager W. F., Korzekwa K. R. (1994) Impaired (S)-warfarin metabolism catalysed by the R144C allelic variant of CYP2C9. *Pharmacogenetics* **4**, 39-42.

Ridderström M., Masimirembwa C., Trump-Kallmeyer S., Ahlefelt M., Otter C., Andersson T. B. (2000) Arginines 97 and 108 in CYP2C9 are important determinants of the catalytic function. *Biochem. Biophys. Res. Commun.* **270**, 983-7.

Rosemary J., Surendiran A., Rajan S., Shashindran C. H., Adithan C. (2006) Influence of the CYP2C9 AND CYP2C19 polymorphisms on phenytoin hydroxylation in healthy individuals from south India. *Indian J. Med. Res.* **123**, 665-70.

Störmer E., Brockmöller J., Roots I., Schmider J. (2000) Cytochrome P-450 enzymes and FMO3 contribute to the disposition of the antipsychotic drug perazine in vitro. *Psychopharmacology* **151**, 312-320.

Tai G., Dickmann L. J., Matovic N., Devoss J. J., Gillam E. M. J., Rettie, A. E. (2008) Re-engineering of CYP2C9 to probe acid-base substrate selectivity. *Pharmacology* **36**, 1992-1997.

Tang C., Shou M., Rushmore T. H., Mei Q., Sandhu P., Woolf E. J., Rose M. J., Gelmann A., Greenberg H. E., Lepeleire I. D., Hecken A. V., Schepper P. J. D., Ebel D. L., Schwartz J. I., Rodrigues A. D. (2001) In-vitro metabolism of celecoxib , a cyclooxygenase-2 inhibitor, by allelic variant forms of human liver microsomal cytochrome P450 2C9: correlation with CYP2C9 genotype and in-vivo pharmacokinetics. *Pharmacogenetics* **11**, 223-235.

Tracy T. S., Hutzler J. M., Haining R. L., Rettie A. E., Hummel M. A., Dickmann L. J. (2002) Polymorphic variants (CYP2C9*3 and CYP2C9*5) and the F114L active site mutation of CYP2C9: effect on atypical kinetic metabolism profiles. *Drug Metab. Dispos.* **30**, 385-390.

Tsao C. C., Wester M. R., Ghanayem B., Coulter S. J., Chanas B., Johnson E. F., Goldstein J. A. (2001) Identification of human CYP2C19 residues that confer S-mephenytoin 4'-hydroxylation activity to CYP2C9. *Biochemistry* **40**, 1937-44.

Visser L. E., Vliet M. V., Schaik R. H. N. V., Kasbergen A. A. H., Smet P. A. G. M. D., Vulto A. G., Hofman A., Duijn C. M. V., Stricker B. H. Ch. (2004) The risk of overanticoagulation in patients with cytochrome P450 CYP2C9*2 or CYP2C9*3 alleles on acenocoumarol or phenprocoumon. *Pharmacogenetics* **14**, 27-33.

Vormfelde S. V., Engelhardt S., Zirk A., Meineke I., Tuchen F., Kirchheiner J., Brockmöller J. (2004) CYP2C9 polymorphisms and the interindividual variability in pharmacokinetics and pharmacodynamics of the loop diuretic drug torsemide. *Clin. Pharmacol. Ther.* **76**, 557-66.

Yamazaki H., Inoue K., Shimada T. (1998) Roles of two allelic variants (Arg144Cys and Ile358Leu) of cytochrome P4502C9 in the oxidation of tolbutamide and warfarin by human liver microsomes. *Xenobiotica* **28**, 103-115.

Yasar U., Forslund-Bergengren C., Tybring G., Dorado P., Llerena A., Sjöqvist F., Eliasson E., Dahl M.-L. (2002) Pharmacokinetics of losartan and its metabolite E-3174 in relation to the CYP2C9 genotype. *Clin. Pharmacol. Ther.* **71**, 89-98.

Yasar U., Annas A., Svensson J.-O., Lazorova L., Artursson P., Al-Shurbaji A. (2005) Ketobemidone is a substrate for cytochrome P4502C9 and 3A4, but not for P-glycoprotein. *Xenobiotica* **35**, 785-796.

Yin T., Maekawa K., Kamide K., Saito Y., Hanada H., Miyashita K., Kokubo Y., Akaiwa Y., Otsubo R., Nagatsuka K., Otsuki T., Horio T., Takiuchi S., Kawano Y., Minematsu K., Naritomi H., Tomoike H., Sawada J.-i., Miyata T. (2008) Genetic variations of CYP2C9 in 724 Japanese individuals and their impact on the antihypertensive effects of losartan. *Hypertens. Res.* **31**, 1549-1557.

Zhou Y.-H., Zheng Q.-C., Li Z.-S., Zhang Y., Sun M., Sun C.-C., Si D., Cai L., Guo Y., Zhou H. (2006) On the human CYP2C9*13 variant activity reduction: a molecular dynamics simulation and docking study. *Biochimie* **88**, 1457-65.